TRIBHUVAN UNIVERSITY

INSTITUTE OF ENGINEERING

PULCHOWK CAMPUS

THESIS NO: 079MSMSE012

Synthesis and Electrochemical Characterization of Zinc Cobalt Bimetallic Oxide as an Advanced Positrode Material for Supercapacitor Application

BY

Rabin Chakatu

A THESIS

SUBMITTED TO DEPARTMENT OF APPLIED SCIENCES AND CHEMICAL ENGINEERING AS A PARTIAL FULFILLMENT OF THE REQUIREMENTS FOR THE DEGREE OF MASTER OF SCIENCE IN MATERIAL SCIENCES AND ENGINEERING

DEPARTMENTOF APPLIED SCIENCES AND CHEMICAL ENGINEERING

LALITPUR, NEPAL

NOVEMBER 2025

COPYRIGHT

The author has agreed that the library, Department of Applied Sciences and Chemical Engineering, Pulchowk Campus, Institute of Engineering may make this thesis freely available for inspection. Moreover, the author has agreed that permission for extensive copying of this thesis for scholarly purpose may be granted by the professor who supervised the work recorded herein or, in their absence, by the Head of the Department wherein the thesis was done. It is understood that the recognition will be given to the author of this thesis and to the Department of Applied Sciences and Chemical Engineering, Pulchowk Campus, Institute of Engineering in any use of the material of this thesis. Copying or publication or the other use of this thesis for financial gain without approval of the Department of Applied Sciences and Chemical Engineering, Pulchowk Campus, Institute of Engineering and author's written permission is prohibited. Request for permission to copy or to make any other use of the material in this thesis in whole or in part should be addressed to:

Head of Department

Department of Applied Sciences and Chemical Engineering

Pulchowk Campus, Institute of Engineering

Lalitpur, Kathmandu

Nepal

TRIBHUVAN UNIVERSITY

INSTITUTE OF ENGINEERING

PULCHOWK CAMPUS

DEPARTMENT OF APPLIED SCIENCES AND CHEMICAL ENGINEERING

The undersigned certify that they have read, and recommended to the Institute of Engineering for acceptance, a thesis entitled " **Synthesis and Electrochemical Characterization of Bimetallic Oxide as an Advanced Positrode Material for Supercapacitor Applications**" submitted by **Rabin Chakatu (079MSMSE012)** in partial fulfillment of the requirements for the degree of Master in Science of Material Science and Engineering.

Supervisor, Dr. Khem Raj Shrestha
Assist. Prof.
Department of Applied Sciences and Chemical Engineering

External Examiner, Prof. Dr. Armila Rajbhandari (Nyachhyon)
Central Department of Chemistry
Tribhuvan University, Nepal

Prof. Dr. Sahira Joshi
Head of Department
Department of Applied Sciences and Chemical Engineering

November 25, 2025
Date of Final Thesis Defense

ABSTRACT

Facile cost-effective hydrothermal method successfully employed for synthesis of bimetallic oxides. XRD spectrum analysis confirmed spinel crystalline phase $ZnCo_2O_4$ nanoparticles with crystallites size expected to be in range of ~35 nm which aligns with the typical morphology of spinel $ZnCo_2O_4$ and FESEM of particle shows sea urchin like morphology with radially projecting nanoneedles structure. Electrochemical performance is studied in three- electrode system using 6M KOH electrolyte solution. $ZnCo_2O_4$ exhibits best specific capacitance of 864.18 Fg^{-1} compared to $CoZn_2O_4$ with 779.18 Fg^{-1}, this slightly less value is due to fewer accessible Co active sites as they are replaced by Zn^{2+} and both bimetallic show superior performance compared to ZnO and CoO with Cs 668.43 Fg^{-1} and 522.68 Fg^{-1} respectively at 1 Ag^{-1} current density. This is due to two metals Zn and Co interact electronically creating new energy states and multiple oxidation states as Co ions show $Co^{2+}/Co^{3+}/Co^{4+}$ transitions whereas Zn^{2+} stabilizes the lattice and enhances more electron mobility and exchange. In EIS analysis $ZnCo_2O_4$ shows least Rct value of ~0.3 Ohm compared to $CoZn_2O_4$ ~0.33 Ohm and highest value for CoO of ~0.52 Ohm, hence $ZnCo_2O_4$ shows rapid electron transport and enhanced redox activity. Both $ZnCo_2O_4$ and $CoZn_2O_4$ show excellent rate capability with specific capacitance retention more than 50% in higher current density of 20 Ag^{-1} compare to only 38% and 30% retention for ZnO and CoO respectively. $ZnCo_2O_4$ shows excellent cyclic stability maintaining 71% of its capacitance after 4,000 GCD cycles at 20 Ag^{-1} current. This improved performance results from the synergistic redox activity of Zn and Co, enhanced electron transport, and optimized porous morphology that favours ion diffusion. This paper demonstrates $ZnCo_2O_4$ characteristics are better than previously reported data making it as an effective positive electrode material for high-capacity supercapacitors.

Keywords: Bimetallic Oxides, Specific Capacitance, Positive Electrode, Supercapacitor, Nanoparticles

ACKNOWLEDGEMENT

I am so grateful with my sincere appreciation to my supervisor/mentor Dr. Khem Raj Shrestha for his persistent and valuable guidance, support and encouragement throughout this research. His support and expertise have been essential in completing this work, without this it wouldn't been completed. I want to thanks program coordinator Assist. Prof. Dr. Ganesh Kumar Shrestha and Head of Department Prof. Dr. Sahira Joshi.

I would like to extend my thanks to Assist. Prof. Dr. Tanka Mukhiya, Assoc. Prof. Dr. Deval Prasad Bhattarai, Prof. Dr. Hem Raj Pant, Prof. Dr. Gokarna Bahadur Motra, Purnima Mulmi, Rajesh Shrestha for their support and encouragement. I like to extend my thanks to Roshna Shrestha for lab support and my colleague Er. Kalyan Karakheti and Er. Ashman Karki for their helps in my work at lab. Also, I am grateful to Department of Applied Sciences and Chemical Engineering, Pulchowk Campus for providing the resources and a conducive environment for my research work.

Lastly, I would like to acknowledge all the researchers for their articles which I have used in writing this thesis.

CONTENTS

LIST OF FIGURES

LIST OF TABLES

LIST OF ABBREVIATIONS AND SYMBOLS

ABBREVIATIONS

AC	Activated Carbon
AFM	Atomic Force Microscopy
BMOs	Bimetallic Oxides
CCDs	Charge Coupled Devices
CE	Counter Electrode
CNTs	Carbon Nanotubes
CV	Cyclic Voltammetry
DI	Deionized Water
ECs	Electrochemical Capacitors
EDL	Electric Double Layer
EDLCs	Electric Double Layer Capacitors
EDS	Energy Dispersive X-Ray Spectrometry
EES	Electrochemical Energy Storage
EIS	Electrochemical Impedance Spectroscopy
ESR	Equivalent Series Resistance
FE-SEM	Field Emission Scanning Electron Microscopy
FWHM	Full Width at Half Maximum
GCD	Galvanostatic Charge Discharge
HSCs	Hybrid Supercapacitors
JCPDS	Joint Committee on Powder Diffraction Standards
LDH	Layer Double Hydroxide
MMOs	Mixed Metal Oxides
PCs	Pseudocapacitors
PDF	Powder Diffraction File
PVDF	Polyvinylidene Fluoride
RE	Reference Electrode
SCs	Supercapacitors
SEM	Scanning Electron Microscopy
SS	Stainless Steel
SSA	Specific Surface Area
TEM	Transmission Electron Microscopy
TMOs	Transition Metal Oxides
WE	Working Electrode
XRD	X-Ray Diffraction

SYMBOLS

° C	Degree celcius
2D	Two dimensional
Cs	Specific capacitance
Ed	Energy density
F	Faraday
M	Molar mass
mg	Milligram
mL	Milliliter
mm	Millimeter
mmol	Milimole
Pd	Power density
pH	Potential of hydrogen
Rct	Charge transfer resistance
Rs	Solution resistance
s^{-1}	Per second
V	Voltage
Wo	Warburg Impedance
Z	Impedance
Z'	Real part of Impedance
Z"	Imaginary part of Impedance
µL	Microliter

CHAPTER 1: INTRODUCTION

1.1 Background of study

Researchers are worried about the fossil fuels consumption as main energy source, it is depleting, causing harsh environmental pollutions, water, air, soil have been degradating, causing impacts in human health, agriculture, drinking water depletion, wildlife and forests depletion ultimately destroying ecosystems. Hence focus on renewable sources of energy is inevitable, but these sources need storage devices (Prabhakar Vattikuti et al., 2023). Worldwide increasing consumption of energy points towards risk of global energy crisis, this comes environment, economic, political, and social concerns (Zameer et al., 2023). As report shows 81% of total energy comes from dominant fossil fuel (Abbasi et al., 2020). Increasing world's population which predicted to rise from 7 to 9 billion by 2050 demands energy, which simultaneously predicted to skyrocket from 12.5 to 16 billion tons of oil equivalent (Al-Obaidi & NguyenHuynh, 2018). By 2030 international energy consumption will jump by 53% (Zeghlouli et al., 2021). Only sustainable and ecofriendly energy solutions will overcome and fulfil the limitation and demand of energy (Al-Obaidi & NguyenHuynh, 2018).

Energy is foundation of modern society. Industrialization and power consumption indicates how developed and modern is the society, electrical energy utilized by various systems, industries, and devices per time shows level of development (Biswas et al., 2024). That forces to have sufficient, efficient, sustainable, clean and secure energy sector. Recent developments in renewable and sustainable energy sources like wind and solar power paves path towards future, as this increases complexity in power distribution systems and discrete power generation. This leads to invention of advanced large scale energy storage systems. These storage systems works based on principal of mechanical, chemical, electrical and electrochemical (J. Liu et al., 2018). Among these electrochemical energy storage (EES) systems are more advance implode in electrochemical capacitors (ECs) and batteries. In comparison EES shows high cyclic efficiency, long cycle life and wide range of implementation. Recent trend in supercapacitor which has exceptional power density (Pd), fast charge–discharge capability, and extended cycle life, make supercapacitor ideal system for next-

generation hybrid energy storage systems, applicable in vehicular and stationary energy storage (González et al., 2016).

Supercapacitors show atypical power density, rapid charge-discharge rates, and long lasting cycle life, this mitigates the drawbacks and limitations of traditional capacitors and batteries needed for modern application. But the electrode material used in supercapacitor has narrow working potential window and low energy density, this limits its application (Kumar et al., 2024).

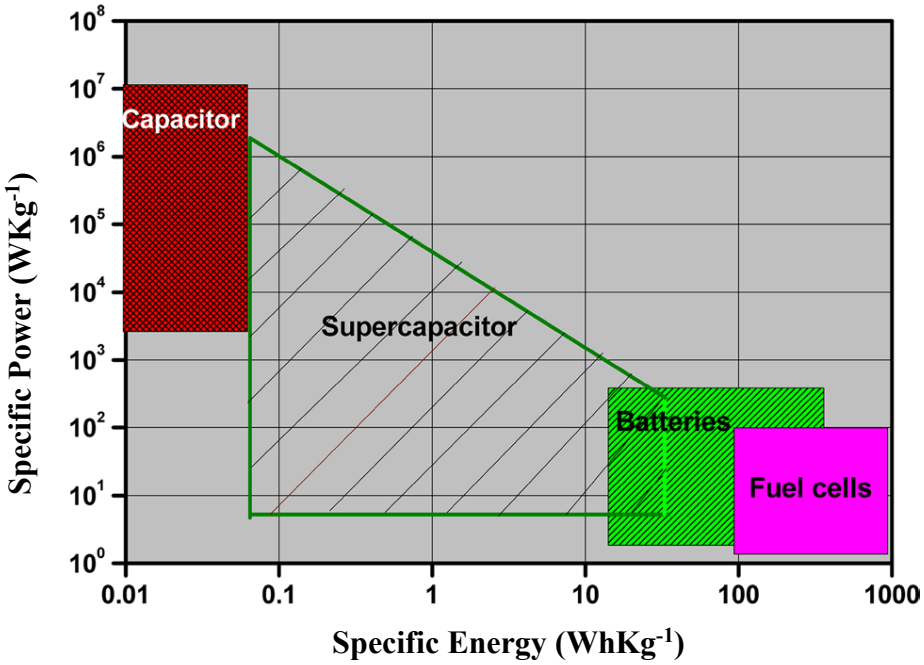

Figure 1. Ragone Plot for electrical energy storage devices (specific energy against specific power) (Lokhande et al., 2020)

This study tries to work on path of sustainable, efficient, and scalable energy storage, by synthesis and characterization of advanced electrode materials for electrochemical energy storage. By exploring novel electrode materials of metal oxides, the study aims to impact to field of knowledge required for the advance energy storage systems.

Table 1. Comparison between batteries and supercapacitors (González et al., 2016)

Parameter	Battery	Supercapacitor
Storage Mechanism	Chemical	Physical

Power Limitation	Reaction kinetics, mass transport	Electrolyte conductivity
Energy Storage	High (bulk)	Limited (Surface area)
Charge Rate	Kinetically limited	High, same as discharge
Cycle life limitation	Mechanical stability, chemical reversibility	Side reactions

1.2 Supercapacitor materials and devices

Electrode materials can be classified whether their electrochemical data correspond to a battery or a supercapacitor. Battery-type electrode presents CVs with defined oxidative and reductive peaks and flat (plateau) galvanostatic charge/discharge (GCD) profiles. Electrode's nature is analysed by nature of current versus scan rate curves. In battery-type electrode materials, the peak current (i) is proportional to the square root of the scanning rate ($i \sim v^{1/2}$), and for a capacitor-like electrode the current will be proportional to the scan rate ($i \sim v$) (Gogotsi & Penner, 2018).

Bases on charge storage mechanisms, supercapacitors are classified into two types: electro- chemical double-layer capacitors (EDLCs) and pseudo-capacitors (PCs). EDLCs store charge through non- faradaic process by developing electrochemical double layers at the electrode/electrolyte interface. Whereas, in case of pseudocapacitors, the electrochemical behaviour is partially capacitive and faradaic (like batteries (Gonçalves et al., 2022).

1.3 Types of Supercapacitors

Supercapacitors are categorized into three types based on their charge storage mechanism:

a. Electric Double-Layer Capacitors (EDLCs)

Electric Double Layer Capacitors (EDLCs) store electrical energy through the physical, electrostatic accumulation of ions at the electrode electrolyte interface when voltage is applied. This process is non-faradaic without any chemical reactions allowing much faster charging and discharging (Zhi et al., 2013). It shows extended stability in charge-discharge cycles, this is due high reversibility in charge storage without suffering volume or structure disintegration (Vangari et al., 2013). Carbon-based materials like graphene, activated carbon, and carbon nanotubes (CNTs) are widely researched electrode material for EDLCs (Askari et al., 2021). The specific capacitance for Electric Double Layer Capacitors (EDLCs) can be measured using the following equation.

$$C = \frac{\epsilon_r \epsilon_o}{d} A \qquad \text{……..(1)}$$

Where, ϵ_r is the relative permittivity of the medium in the EDL, ϵ_o is the permittivity of the vacuum, A is the specific area of the electrode, and d is the thickness of the EDL. Despite their long cycle life it exhibits low energy density, making their potential applications as energy storage challenging (Lokhande et al., 2020).

b. Pseudocapacitors

In other hand, pseudocapacitors work on fast, reversible faradaic redox reactions at the electrode surface, giving them significantly enhances charge storage capacity compared to EDLCs (González et al., 2016). Here, charge generated through redox reactions, which then transfer across the double layer as shown in **Figure 2.** (b). This faradaic mechanism can be divided into three types,

i) Reversible adsorption
ii) Redox reaction occurring in metal oxides
iii) Reversible doping/ de- doping electrochemical process in conductive polymer- based electrodes (Shi et al., 2014).

Pseudocapacitors show higher specific capacitance and energy density than that of EDLCs due to faradaic reactions occurring not only at the surface of electrode, but also near the surface of electrodes (Iro et al., 2016). Theoretical capacitance can be calculated using following equation:

$$C = \frac{nF}{MV} \qquad \text{……..(2)}$$

where n is the number of electrons transferred in the faradaic reaction, F is Faraday constant, M is the molar mass of the active material and V is the Potential window (Lokhande et al., 2020).

Transition metal oxides (TMOs) such as MnO_2, Co_3O_4, and NiO are widely studied pseudocapacitive materials (Balaji et al., 2021). Redox mechanism causes volume change during charge/ discharge cycle, this phenomenon causes lower cycling lifespans and poor mechanical/ structural stability (González et al., 2016).

c. Hybrid Supercapacitors (HSCs)

Hybrid Supercapacitors combine both EDLCs and pseudocapacitors property by integrating carbon-based materials with redox-active TMOs (Pawar et al., 2019). Hybrid configurations enable improved energy density and cycling stability, making them attractive candidates for next-generation energy storage systems.

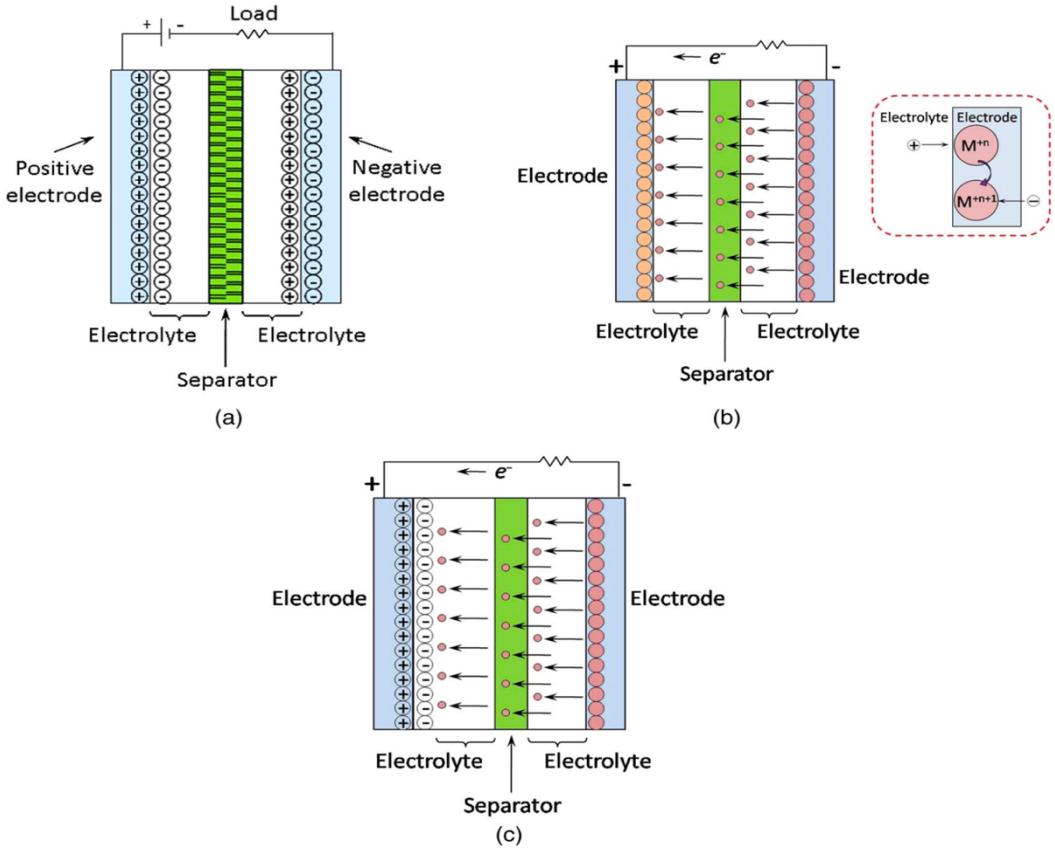

Figure 2. Schematic diagram of supercapacitors: a) EDLC type, b) Pseudocapacitor type, c) Hybrid type ((Vangari et al., 2013)

Table 2. Difference between EDLC, Pseudocapacitor and Hybrid Capacitor (Zhang et al., 2009)

Parameters	EDLC	Pseudocapacitor	Hybrid capacitor
Storage mechanism	Non-faradaic/electrostatic, electrical charge stored at the metal/electrolyte interface	Faradaic, reversible redox reaction	Faradaic and non-faradaic
Specific capacitance	Lower	Higher	Higher
Energy density	Low	High	High
Cyclic Life	High	Low	High
Material	Carbon- based materials- activated carbon, carbon nanotubes	Metal oxides, conducting polymers, NiO, MgO, PANI	Metal Oxide/carbon-based materials, conducting polymer/carbon-based material, $Ni(OH)_2$/rGO, PANI/rGO

1.4 The Electrodes and Electrolytes in Supercapacitors

The Electrodes

Supercapacitor electrodes typically consist of thin coatings of active material electrically integrated with a conductive metallic current collector. These electrodes must exhibit a combination of critical properties, including thermal stability, excellent electrical conductivity, chemical inertness, high specific surface area (SSA), corrosion

resistance, environmental compatibility, and cost-effectiveness for ensuring long-term performance and reliability under varying operational conditions (Molahalli et al., 2024). The electrochemical performance of electrode materials is strongly influenced by their ability to facilitate Faradaic charge transfer, which significantly enhances the specific capacitance (Cs) of the device. Moreover, reducing the pore size of the electrode material can increase both Cs and energy density (Ed) by promoting efficient ion access and storage. However, excessively small pores may lead to increased equivalent series resistance (ESR), which can in turn reduce the power density (Pd) of the device due to hindered ion transport.

Recent advancements in supercapacitor electrodes include a broad range of material systems such as graphene and its derivatives, transition metal oxides and hydroxides, carbon-based materials, two-dimensional (2D) nanostructures, conducting polymers, and various hybrid and composite materials. In addition, innovations in ionic liquids and gel-based electrolytes are being explored to further enhance the electrochemical performance and safety of supercapacitor devices (Kumar et al., 2024).

The Electrolytes

Electrolytes are a crucial component of supercapacitors, which conduct ions between the electrodes, defining the energy density, power density, cyclic stability, and efficiency of the devices. Its other characteristics are a wide electrochemical voltage window, high electrochemical stability, high ionic concentration, low solvated ionic radius, low viscosity, low volatility, low toxicity, cost-effectiveness, and availability in high-purity form, which affect device capacitance (Mendhe & Panda, 2023).

Additionally, electrode and current collector corrosion is a critical factor influenced by the electrolyte's composition, and in the case of aqueous electrolytes, by the pH. Therefore, it is essential to conduct a preliminary electrochemical stability assessment for each specific electrode–electrolyte combination to ensure safe, reversible, and long-term operation of the final device (González et al., 2016). Major electrolytes for supercapacitors are classified into three categories: a) aqueous electrolytes, b) organic electrolytes, and c) ionic liquid (Khan et al., 2021).

1.5 Electrode Material Fabrication Methods

There has been practised different types of methods used in synthesis of supercapacitor electrode material. Like electrochemical deposition, chemical bath deposition, chemical vapour deposition, the sol- gel method, and hydrothermal method.

Hydrothermal Method

The hydrothermal method is one of the most widely employed techniques for the synthesis of nanomaterials, owing to its versatility and effectiveness in controlling particle morphology and composition. This method is based on solution-phase reactions conducted within a sealed autoclave, where a wide range of temperatures, from room temperature up to several hundred degrees Celsius can be applied. One of the key advantages of the hydrothermal process is its ability to produce nanomaterials that are thermally stable at high temperatures, thus preserving their structural integrity. Additionally, the method offers minimal material loss and enables precise control over the composition and crystallinity of the resulting nanostructures through well-regulated liquid-phase or multiphase chemical reactions. Various nanostructures such as nanoparticles, nanorods, nanotubes, hollow nanospheres, and graphene nanosheets have been successfully synthesized using hydrothermal techniques, demonstrating its broad applicability in nanomaterials research. Hydrothermal synthesis method was employed for synthesis of various Co-doped $Zn_{1-x}Co_xMn_2O$ nanocrystals with a spinel structure forming hollow nanospheres (Gan et al., 2020).

1.6 Electrochemical Evaluation Techniques

Supercapacitor characterization is typically performed using an electrochemical workstation (EW), which integrates a potentiostat, galvanostat, and, optionally, a frequency response analyser for electrochemical impedance spectroscopy (EIS). In potentiostatic mode, the system precisely controls the potential of the counter electrode (CE) relative to the working electrode (WE), while monitoring the resulting current response. Conversely, in galvanostatic mode, a constant current is maintained between the working and counter electrodes, and the corresponding voltage response is recorded.

Two main cell configurations are employed to evaluate supercapacitor performance: the three-electrode and two-electrode systems. The two-electrode configuration closely replicates the actual operating conditions of a full supercapacitor device, as both electrodes contribute to the overall capacitance. This setup is commonly used for reporting device-level performance metrics such as specific capacitance (Cs), energy density (Ed), and power density (Pd). On the other hand, the three-electrode configuration is utilised for fundamental investigations of electrode materials. In this setup, the response is solely due to the working electrode under study, while the reference electrode provides a stable potential against which the WE are measured, and the CE completes the circuit. This arrangement allows for accurate analysis of the electrochemical behaviour of individual materials, without interference from a second electrode. While it is relatively straightforward to analyse individual electrodes in symmetric devices using a two-electrode setup, this becomes challenging in asymmetric supercapacitors, where the electrodes are made of different materials. The two-electrode configuration does not allow for precise attribution of performance to each electrode in such systems. Therefore, for asymmetric configurations, the three-electrode setup is preferred when studying individual electrode performance (Khan et al., 2021).

a. Cyclic Voltammetry (CV)

Dynamic method for evaluating electrochemical capabilities of a device or material through electrode kinetics and charge storage mechanism happening at the electrode/electrolyte interface. 2 or 3 electrode configurations used, working electrode potential is measures against a reference electrode which maintains a constant potential. Distinct shape CV graphs are generated (rectangular/quasi-rectangular), with time-dependent current on the vertical axis and predetermined voltage window on the horizontal axis, when a fixed rate linear varying voltage is swept between two predetermined upper and lower electric potential values. The scan is forwarded and reversed between this voltage bracket, also known as operating potential or voltage window. This voltage window value depends upon the type of electrolyte used, as the voltage range should not surpass the stable voltage operating window of the electrolyte.

Exceeding the voltage limit will start the electrolysis process of an electrolyte, and this reaction will govern the cell chemistry, thus resulting in deteriorated cell performance. Different scan rates (mV/s) are also employed during CV analysis; this voltage/potential change speeds during the experimental setup. The scan rate has a considerable impact on capacitance values and graphs obtained. It is mainly related to electrode kinetics, as the decrease in specific capacitance is associated with limited ion transfer due to increased scan rate. At slower scan rates, the CV graphs also show better rectangular charts. Eq. (7) can be used to calculate the capacitance values of a super cache capacitor when the CV technique is used in two-electrode assemblies (Khan et al., 2021).

b. Galvanostatic charge- discharge (GCD)

GCD is another most widely utilized electrochemical techniques for evaluating the performance of supercapacitor devices and electrode materials. It provides direct insights into key parameters such as capacitance, energy density, power density, and equivalent series resistance (ESR). Moreover, GCD testing plays a crucial role in assessing the long-term cycling stability and life cycle performance of a supercapacitor. In a typical GCD experiment, a constant current is applied to the working electrode to charge the device up to a predefined voltage (as determined by the voltage window), and the voltage response is recorded over time. Following full charge, a reverse current of equal magnitude is applied to discharge the device, and the voltage drop is monitored accordingly.

The resulting GCD profile typically exhibits a symmetrical triangular shape, characteristic of ideal capacitive behaviour in supercapacitors. Deviations from linearity can indicate resistive losses or pseudocapacitive contributions. The slope of the charge/discharge curve is directly related to the capacitance of the device, and the IR drop observed at the beginning of discharge provides insight into the internal resistance of the cell (Khan et al., 2021).

c. Electrochemical impedance spectroscopy (EIS)

Electrochemical Impedance Spectroscopy (EIS) is a powerful diagnostic technique that provides detailed information about the electrochemical behaviour of supercapacitor

devices. It offers insights into critical phenomena such as impedance, frequency response of capacitance, and interfacial processes at the electrode/ electrolyte boundary, including charge transfer resistance and mass transport limitations. Also referred to as AC impedance spectroscopy or dielectric spectroscopy, EIS is conducted by superimposing a small-amplitude AC signal- either voltage (potentiostatic mode) or current (galvanostatic mode) onto a steady-state signal across a broad frequency range. The system's impedance response to this perturbation is then analysed to understand both resistive and capacitive elements of the electrochemical cell.

The output of an EIS experiment is typically presented in the form of a Nyquist plot, which depicts the real (Z') and imaginary (Z'') components of the device impedance. The high-frequency intercept on the real axis corresponds to the solution resistance, while the semicircle observed at mid frequencies indicates charge transfer resistance, and the low-frequency tail represents diffusive or capacitive behaviour. The specific capacitance of the system can also be extracted using the imaginary part of the impedance. Thus, EIS serves as a comprehensive technique to assess the dynamic electrochemical performance and internal resistance characteristics of supercapacitor systems (Khan et al., 2021).

1.7 Morphological Characteristic

Nanostructured materials represent a novel class of materials that have garnered substantial attention due to their remarkable potential across various advanced technological applications, including electronics, optics, magnetic data storage, energy storage and harvesting, and catalysis. These materials are broadly categorized into nanostructured materials and nanophase or nanoparticles. Unlike their bulk counterparts, nanomaterials exhibit distinct physicochemical properties arising from their reduced dimensions and enhanced surface effects. Critical parameters such as particle size, shape, surface structure, and interparticle interactions significantly influence their performance and behaviour. To comprehensively understand the role of nanomaterials in nanoscience and nanotechnology, it is essential to examine the internal structure, morphology, and distribution of nanostructures. This understanding can be effectively achieved through advanced morphological characterization techniques, including electron microscopy (such as TEM and SEM), optical microscopy, and

scanning probe techniques like AFM. These tools provide critical insights into the nanoscale features and help establish a clear distinction between bulk and nanostructured materials, which is fundamental for tailoring their properties for specific applications (Mayeen et al., 2018).

1.8 Structural Characteristic

X-ray Diffraction (XRD) is a widely employed analytical technique primarily used to determine the crystal structure and phase composition of materials, particularly at the nanoscale. The technique is based on the interaction of X-ray beams with the crystal lattice of a material. Since the typical interatomic distances in crystalline substances range from 2–3 Å, which corresponds well with the wavelength of X-rays, diffraction occurs when these beams are incident on the lattice planes at specific angles. This results in both constructive and destructive interference patterns, forming a diffraction spectrum that provides insights into the crystal symmetry, lattice parameters, and crystallite size. Different types of detectors, including photographic film, imaging plates, and charge-coupled devices (CCDs), are utilized to record the diffraction patterns, which are then converted into digital data for analysis. XRD has proven to be highly effective for structural investigation of nanoparticles, as demonstrated in several studies (Anandharamakrishnan, 2013).

1.9 Organization of Dissertation

Chapter 1. This section manifests the background of study, introduction and motivation for this research project.

Chapter 2. This chapter presents the literature review on the bimetallic oxide preparation techniques, characteristics, fundamentals and working principle of supercapacitors, electrolyte and electrode material in supercapacitors, electrochemical evaluation techniques, and potential of Zinc Cobalt bimetallic oxide as positive electrode material for application in supercapacitor.

Chapter 3. Objectives of this research study.

Chapter 4. This chapter includes the details materials and methodology used and performed for material synthesis and characterization.

Chapter 5. This chapter discusses the physiochemical characterization and analysis of electrochemical experiments.

Chapter 6. This chapter conclude the results and summary and limitation and possibilities of future scope of study.

CHAPTER 2: LITERATURE REVIEW

Electrode material morphology, i.e. the form and size of the pores and chemical affinity towards deposited ions on the electrode surface is proportional to the capacity of electrodes pseudo capacitance. Some transition metal oxides like Iron oxide, Nickel Oxide, Vanadium Oxide, MnO_2, and Co_3O_4 are used in pseudocapacitors due to their redox behaviour (Rudra et al., 2024). Transition metal oxides exhibit multiple oxidation states, enabling efficient charge storage through redox reactions. Common TMOs used in supercapacitors include MnO_2, NiO, Co_3O_4, and Fe_2O_3 (Askari et al., 2021). These materials offer high theoretical capacitance but suffer from inherent drawbacks such as low electrical conductivity and limited cycling stability (Balaji et al., 2021). To overcome these limitations, researchers have explored nanostructured TMOs, composite materials, and doping strategies to enhance their electrochemical performance (Pawar et al., 2019). Among BMOs, zinc-cobalt oxide ($ZnCo_2O_4$) has emerged as a promising electrode material due to its superior electrical conductivity, high theoretical capacitance (~2650 F/g), and excellent stability (Tiwari et al., 2021). Recent studies have demonstrated that $ZnCo_2O_4$ nanostructures synthesized via hydrothermal and sol-gel methods exhibit remarkable electrochemical performance (Pawar et al., 2019).

This study explored the hydrothermal synthesis of $ZnCo_2O_4$ nanoparticles. It aimed to optimize the bimetallic oxide by modifying the precursor mixing concentration with urea as an assistant for surface microstructure and evaluating its electrochemical performance.

2.1 Importance of Electrode Materials in Supercapacitor Performance

- The performance of supercapacitors is largely dictated by the properties of the electrode materials. Ideal electrodes must exhibit high electrical conductivity, a large surface area, excellent redox activity, and mechanical stability to sustain prolonged cycling (Balaji et al., 2021). Carbon-based materials, conducting polymers, and transition metal oxides have been extensively investigated for this purpose (Pawar et al., 2019).

- Governing factors for the energy density of devices are potential window, pore size distribution, surface area, electrolytes, and device configurations (Balaji et al., 2021).
- Among these, transition metal oxides (TMOs) stand out due to their ability to store charge through Faradaic reactions, significantly enhancing specific capacitance. However, single-component TMOs often face limitations such as low electrical conductivity and volume expansion during cycling, leading to structural degradation. This has led to growing interest in bimetallic oxides, which offer synergistic benefits by incorporating two metal species into a single oxide matrix (Yewale et al., 2025b)

2.2 Transition Metal Oxides (TMOs) and Their Role in Energy Storage

Transition metal oxides exhibit multiple oxidation states, enabling efficient charge storage through redox reactions. Common TMOs used in supercapacitors include MnO_2, NiO, Co_3O_4, and Fe_2O_3 (Askari et al., 2021). These materials offer high theoretical capacitance but suffer from inherent drawbacks such as low electrical conductivity and limited cycling stability (Balaji et al., 2021). To overcome these limitations, researchers have explored nanostructured TMOs, composite materials, and doping strategies to enhance their electrochemical performance (Pawar et al., 2019).

Emergence of Bimetallic Oxides as High-Performance Electrode Materials

Bimetallic oxides (BMOs) have garnered significant attention due to their enhanced electrochemical properties compared to monometallic oxides. The incorporation of two metal cations into a single oxide matrix provides several advantages:

- **Synergistic Redox Activity:** Multiple oxidation states facilitate improved charge storage and electron transfer kinetics (Balaji et al., 2021).
- **Enhanced Electrical Conductivity:** The interaction between two metal species can reduce charge transfer resistance, improving overall conductivity (Pawar et al., 2019).

- **Structural Stability:** Bimetallic oxides exhibit improved mechanical integrity, reducing volume expansion and structural degradation during cycling (Askari et al., 2021).

Bimetallic metal oxides spinel cobalties MCo_2O_4 (M= Mn, Ni, Cu, or Zn) are much attractive as they can store large quantity of charges due to their multiple oxidation states, like nickel cobaltite ($NiCo_2O_4$) exhibits two orders of magnitude of higher electrical conductivity than nickel oxide (NiO) or cobalt oxide (Co_3O_4). These metal oxides are superior electrode materials for supercapacitors due their crystal structure (has multiple lattice sites which enhance the performance and stability of electrode material) , defects (like Schottky and Frenkel defects- increases conductivity due to crystal lattice distortion caused by vacancy which changes the lattice vibration) , spin, electronic structure, and synergetic effect (Balaji et al., 2021).

Co- Based Bimetallic Oxides

Cobaltite formed when other transition metal oxides mixed with cobalt which shows superior electrochemical behaviour. Application as electrode materials in electrocatalysis, Li-ion batteries and in supercapacitors. Low cost, abundancy and non-toxicity of these materials and improved reversible capabilities, structural stability, electrical conductivity and high theoretical specific capacities make them ideal for electrode material (Lalwani et al., 2019). Cobalt in trivalent atom result in cobalities like $NiCo_2O_4$, $ZnCo_2O_4$, $MnCo_2O_4$, $FeCo_2O_4$, $CuCo_2O_4$ etc. among these bimetallic oxides combinations Nickel Cobalt is preferred for their high theoretical specific capacity and reversible redox nature (Y. Liu et al., 2018).

Among other BMOs, zinc-cobalt oxide ($ZnCo_2O_4$) has emerged as a promising electrode material due to its superior electrical conductivity, high theoretical capacitance (~2650 F/g), and excellent stability (Yewale et al., 2025b). Recent studies have demonstrated that $ZnCo_2O_4$ nanostructures synthesized via hydrothermal and sol-gel methods exhibit remarkable electrochemical performance (Pawar et al., 2019). $ZnCo_2O_4$ nanosheets and nanowires have been grown on SS sheet to make working electrode, to have large surface areas and dense mesopores for sufficient active sites for Faradic reactions and short distance ion transfer (Sun et al., 2024).

Transition metal oxides, particularly spinel-structured materials like $ZnCo_2O_4$, have garnered significant attention for their potential in energy storage and conversion applications due to their multifunctional electrochemical properties. Recent advances in the controlled synthesis of $ZnCo_2O_4$ micro- and nanostructures have led to the development of materials with unique morphologies and enhanced electrochemical performance. This has spurred interest in their use as electrode materials in supercapacitors and batteries, where both slurry-cast and binder-free configurations have been explored. Notably, several $ZnCo_2O_4$-based electrodes rank among the top-performing materials in these applications (Gonçalves et al., 2022).

Redox process for the synthesis of $ZnCo_2O_4$

Precursor salts, Zinc Nitrate ($Zn(NO_3)_2$) and cobalt nitrate ($Co(NO_3)_2$) when dissolve in water releases their respective metal cations:

$Zn(NO_3)_2 \rightarrow Zn^{2+} + 2NO_3^-$

$Co(NO3)2 \rightarrow Co^{2+} + 2NO_3^-$

Urea used as precipitating agent which initiates hydroxide formation.

$CO(NH_2)_2 + 3H_2O \rightarrow 2NH_4^+ + CO_3^{2-} + 2OH^-$

These OH^- ions react with Zn^{2+} and Co^{2+} ions, forming mixed precursors hydroxide precipitates to form $ZnCo_2O_4$

$Zn^{2+} + 2OH^- \rightarrow Zn(OH)_2 \downarrow$

$Co^{2+} + 2OH^- \rightarrow Co(OH)_2 \downarrow$

As, Co is present in LDH, spinel-type phases (Co_3O_4, Co_2O_3) or perovskite-like phases may start forming.

The amorphous phase crystallizes into $ZnCo_2O_4$ spinel through redox reactions. For Cobalt- rich systems:

$6\ Co(OH)_2 + O_2 \xrightarrow{\Delta} 2Co_3O_4 + 6H_2O$

Zinc ions (Zn^{2+}) integrate into the spinal lattice, stabilizing the structure:

$$Zn^{2+} + 2\ Co^{3+} + 4\ O^{2-} \rightarrow\ ZnCo_2O_4$$

$ZnCo_2O_4$ exhibits a p-type semiconducting nature and shares the spinel crystal structure of Co_3O_4, with Zn^{2+} ions occupying the tetrahedral sites and Co ions residing in the octahedral sites. This cation distribution enriches the material's redox activity, enhancing its electrochemical potential. However, despite these advantages, $ZnCo_2O_4$ suffers from inherently poor electrical conductivity and significant volume changes during charge/discharge processes. These limitations result in increased internal resistance and structural degradation over cycling, leading to rapid capacitance fading at high current densities and poor rate capability and cycling stability, which constrain its practical performance in energy storage devices (Liu et al., 2020).

2.3 Statement of Problem:

Despite significant advancements in research in transition metal bimetallic oxide as an electrode material for supercapacitor, there are limitation in the synthesis of electrode material which is cost effective, simple in operation, and environmentally friendly. Literatures lack the systematic investigation into how precursor concentration and urea assisted hydrothermal synthesis influence its microstructural evolution, defect formation and electrochemical performance. Also with great electrochemical energy storage systems, greater stability and long lasting, high charge–discharge rates with potential in practical applicability and scalability. These limitations hamper the performance of devices like supercapacitors and batteries. Hence, to overcome the limitation in electrode material, there is a critical need to innovate novel electrode material through simple and cost effective, efficient method which can produce novel acceptable electrode material which can be used for energy storage system.

CHAPTER 3: OBJECTIVES

The objectives of this study are listed below:

3.1 General Objective:

1. General objective of this study is to synthesise and characterise bimetallic oxides. the material will be used as advanced positrode materials for supercapacitor applications.

3.2 Specific Objective:

The specific objectives of the study are:

1. Synthesis of Zn-Co bimetallic oxides using facile hydrothermal process.
2. Characterization of as prepared materials by using X-ray diffraction (XRD), Field emission scanning electron microscopy (FE-SEM), Energy- dispersive X-ray spectrometry (EDS) and Elemental colour mapping to study the structural and morphological properties.
3. Evaluation of the electrochemical performance using cyclic voltammetry (CV), galvanostatic charge-discharge (GCD), and electrochemical impedance spectroscopy (EIS).

CHAPTER 4: MATERIALS AND METHODOLOGY

4.1 Materials and Equipment:

1. **Chemicals:**

a. Zinc nitrate hexahydrate ($Zn(NO_3)_2 \cdot 6H_2O$) [96% AR, Loba Chemie Pvt. Ltd.]

b. Cobalt nitrate hexahydrate ($Co(NO_3)_2 \cdot 6H_2O$) [97% AR, Qualikems Fine Chem Pvt. Ltd.]

c. Urea ($CO(NH_2)_2$), Ammonium fluoride (NH_4F), Ethanol (C_2H_6O)[99% AR], Hydrochloric acid [HCl 35% AR], Iso Propyl Alcohol (C_3H_8O) [99% AR, Central Drug House (P) Ltd.], Potassium Hydroxide [KOH, 85% AR, Fisher Scientific], Polyvinylidene fluoride (PVDF), Carbon Black were used.

d. Nickel foam of 1mm thickness was used to make electrode.

2. **Instruments:** Following instruments have been used during entire experimental works: Magnetic Stirrer, Ultasonic Cleaner, Tube Furnace (Kejia Furnace), Centrifuge Machine (BIOBASE), Oven (Gallenkamp), Electrochemical Workstation (CorrTest), Weighing machine (Explorer OHAUS), Stainless steel Autoclave (Teflon cup).

3. **Apparatus:** Beakers, Volumetric Flask, Conical Flask, Measuring Cylinder, Centrifuge Tubes, Viles, Micropipette, Agate Mortar and pestle were used in process of experiment work.

The chemicals were of analytical grade and used directly as get without any further purification.

4.2 Methods:

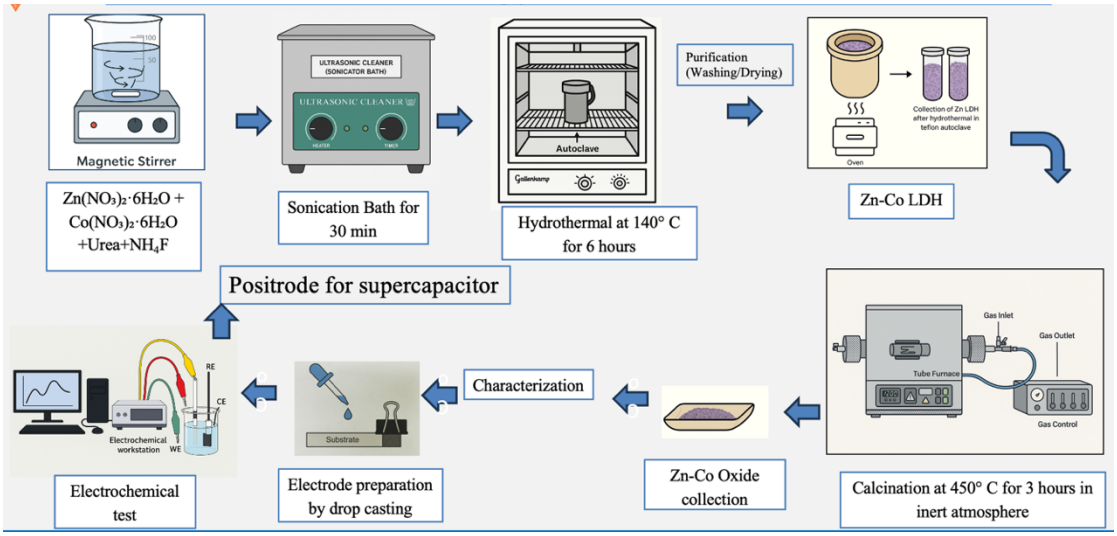

Figure 3. Schematic representation synthesis of bimetallic oxide, characterization

4.2.1 Synthesis of $ZnCo_2O_4$

Step I: Preparation of precursor solution

In this step precursors 1 mmol $Zn(NO_3)_2 \cdot 6H_2O$ and 2 mmol $Co(NO_3)_2 \cdot 6H_2O$ were dissolved in 25 mL of deionized water separately under continuous stirring to ensure complete dissolution. Then 25mL dissolved $Co(NO_3)_2 \cdot 6H_2O$ solution was added to the solution of $Zn(NO_3)_2 \cdot 6H_2O$ drop wise with continuous stirring in time span of 5 minutes. Similarly, after mixing precursors, $CO(NH_2)_2$ in molar ratio of 1:2 (Metal: Urea) was introduced as a precipitating agent to regulate pH and facilitate uniform hydroxide formation. The 15mL 6 mmol urea solution was prepared in beaker then added in the mixture in time span of 10 minutes drop by drop. Finally, 5mL 2 mmol NH_4F was incorporated to control morphology and enhance surface area. Afterward, solution was magnetically stirred at room temperature for 30 minutes, ensuring homogeneity and assisted by 15 minutes sonication. The final mixture was then transferred to 100mL autoclave Teflon cup, then kept in oven at 140 degrees Celsius for 6 hours for hydrothermal process.

Step II: Hydrothermal Method

The prepared precursor solution was transferred to a 100 mL Teflon-lined stainless-steel autoclave and subjected to hydrothermal treatment at 140°C for 6 hours after

elevation of temperature to required. This process enabled the formation of Zn Co-layered double hydroxides (LDH) as an intermediate phase. After completion, the autoclave was naturally cooled to room temperature, and the precipitate obtained was collected. The sample was washed three times with deionized water and ethanol to remove residual impurities and then dried in an oven at 60°C for 12 hours. Here, Urea was used as a precipitating agent to facilitate the formation of the hydroxide precursor. Use of Urea facilitate pH adjustment which improves nucleation and growth of the $ZnCo_2O_4$ crystals (Tiwari et al., 2021).

Figure 4. Precursor solution preparation, Hydrothermal synthesis and ZnCo LDH

Step III: Thermal Calcination process

To obtain $ZnCo_2O_4$, the dried hydroxide precursor was subjected to calcination at 450°C for 3 hours in an inert atmosphere. Ramping temperature was maintained to increase the heating rate 10°C/min and soaking time for 3 hrs at constant temperature of 450°C

Figure 5. Heat annealing in Tube Furnace with Nitrogen atmosphere

and sample was left for controlled cooling at room temperature. This thermal treatment converted the layered double hydroxides into a stable spinel $ZnCo_2O_4$ phase while enhancing crystallinity and improving electrochemical properties. In this process Zn Co LDH was transformed into bimetallic oxide (Zn Co Oxide).

In the process of thermal calcination process following changes took place:

Firstly at ~ 200–300 °C, dihydroxylation process took place in which hydroxyl groups (OH^-) in its layers started to decomposed into H_2O, hence LDH layered structure collapsed. Then anion decomposition took place at ~300–450 °C, in this stage, available carbonate (CO_3^{2-}), nitrate (NO_3^-), or sulphate (SO_4^{2-}) which present as interlayer anions started to decomposed into CO_2, NO_x, or SO_x gases. From this stage leads to formation of metal oxides or oxyhydroxides. Finally mixed metal oxides were formed at ~350–450 °C, LDH converted into mixed metal oxides (MMOs).

4.2.2 Synthesis of $CoZn_2O_4$

Step I: Preparation of Precursor Solution

In this step precursors 2 mmol $Zn(NO_3)_2 \cdot 6H_2O$ and 1 mmol $Co(NO_3)_2 \cdot 6H_2O$ were dissolved in 25 mL of deionized water separately under continuous stirring to ensure complete dissolution. Then 25mL dissolved $Co(NO_3)_2 \cdot 6H_2O$ solution was mixed with solution of $Zn(NO_3)_2 \cdot 6H_2O$ drop wise with continuous stirring in time span of 5 minutes. Similarly, after mixing precursors, $CO(NH_2)_2$ in molar ratio of 1:2 (Metal: Urea) was introduced as a precipitating agent to regulate pH and facilitate uniform hydroxide formation. The 15mL 6 mmol urea solution was prepared in beaker then added in the mixture in time span of 10 minutes drop by drop. Finally, 5mL 2 mmol NH_4F was incorporated to control morphology and enhance surface area. Afterward, solution was magnetically stirred at room temperature for 30 minutes, ensuring homogeneity and assisted by 15 minutes sonication. The final mixture was then transferred to 100mL autoclave Teflon cup for further experiment.

Step II: Hydrothermal Process

The prepared precursor solution was transferred to a 100 mL Teflon-lined stainless-steel autoclave and subjected to hydrothermal treatment at 140°C for 6 hours. This

process enabled the formation of Co Zn (LDH) as an intermediate phase. After completion, the autoclave was naturally cooled to room temperature, and the precipitate obtained was collected. The sample was washed three times with deionized water and ethanol to remove residual impurities and then dried in an oven at 60°C for 12 hours.

Step III: Thermal calcination Process

To obtain $CoZn_2O_4$, the dried hydroxide precursor was subjected to calcination at 450°C for 3 hours in an inert atmosphere. Ramping temperature was maintained to increase the heating rate 10°C/min and soaking time for 3 hrs at constant temperature of 450°C and sample was left for controlled cooling at room temperature. This thermal treatment decomposes LDH into crystalline $CoZn_2O_4$ oxide. The final product was stored in air tight container for further characterization.

4.2.3 Synthesis of ZnO

Step I: Preparation of precursor solution

For synthesis of ZnO, 2 mmol Zinc nitrate hexahydrate ($Zn(NO_3)_2 \cdot 6H_2O$) was dissolved in 35mL distilled water in 150 mL beaker with continuous stirring in magnetic stirrer (Figure 3.), then after complete dissolution of solution, prepared 4 mmol Urea solution was added drop wise in the time span of 10 minutes with continuous stirring, and finally 2 mmol NH_4F in 10mL solution was added to mixture in 5 minute time span drop by drop for uniform mixing. The mixture was stirred for next 30 minutes continuously, then was sonicated for next 15 minutes.

Step II: Hydrothermal Process

The prepared 70ml precursor solution was transferred to a 100 mL Teflon-lined stainless-steel autoclave and subjected to hydrothermal treatment at 140°C for 6 hours using oven (Figure 3.). After completion, the autoclave was naturally cooled to room temperature, and the precipitate obtained was collected. The sample was washed three times with deionized water and ethanol to remove residual impurities and then dried in an oven at 60°C for 12 hours.

Step III: Thermal calcination Process

To obtain ZnO, the dried hydroxide precursor was subjected to calcination at 450°C for 3 hours in an inert atmosphere using tube furnace (Figure 4.). Ramping temperature was maintained to increase the heating rate 10°C/min and soaking time for 3 hrs at constant temperature of 450°C and sample was left for controlled cooling at room temperature. This thermal treatment decomposes LDH into crystalline Zn oxide. The final product was stored in air tight container for further characterization.

4.2.4 Synthesis of CoO

Step I: Preparation of precursor solution

Lastly for CoO, 2 mmole of Co $(NO_3)_2 \cdot 6H_2O$ was dissolved in 35 mL of distilled water, after complete dissolve solution of 4 mmole Urea in 25 mL of distilled water was added drop wise in 10 minutes time span, finally 2 mmol NH_4F in 10 mL solution was mixed drop by drop to insure uniform mixing for 5 minutes time span. The final mixture for stirred continuously for 30 minutes and then sonicated for next 15 minutes. After sonication mixture was transferred to Teflon autoclave cup for hydrothermal process. For all types of oxide hydrothermal was done at 140° C for 6 hours.

Step II: Hydrothermal process

The prepared precursor solution was transferred to a 100 mL Teflon-lined stainless-steel autoclave and subjected to hydrothermal treatment at 140°C for 6 hours. This process enabled the formation of Cobalt hydroxides as an intermediate phase. After completion, the autoclave was naturally cooled to room temperature, and the precipitate obtained was collected. The sample was washed three times with deionized water and ethanol to remove residual impurities and then dried in an oven at 60°C for 12 hours.

Step III: Thermal Calcination process

To obtain CoO, the dried hydroxide precursor was subjected to calcination at 450°C for 3 hours in an inert atmosphere using tube furnace (Figure 4.). Ramping temperature was maintained to increase the heating rate 10°C/min and soaking time for 3 hrs at constant temperature of 450°C and sample was left for controlled cooling at room temperature. This thermal treatment converted the hydroxides into a crystalline CoO.

4.2.5 Structural and Morphological Characterization

The synthesized material was then characterized using multiple techniques. X-ray diffraction (XRD) was employed to confirm phase purity and crystallinity, Field Emission scanning electron microscopy (FESEM) provided insights into morphology and particle distribution.

Step I: X-Ray Diffraction (XRD)

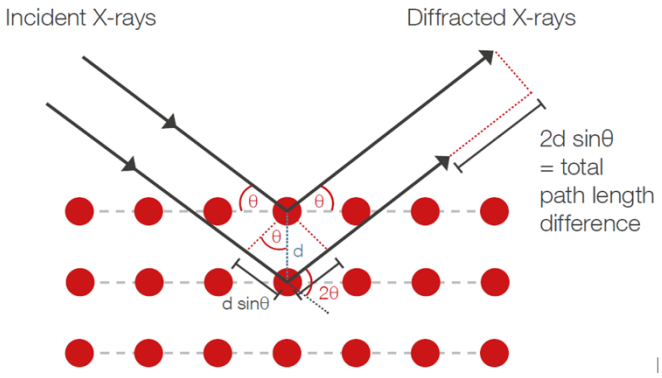

Figure 6. Bragg's Law

Crystal structure was categorized by X- ray diffraction (XRD) technique using Cu Kα radiation (λ = 1.5406 Å). The characteristic diffraction peaks observed at 2θ values obtained in range of (20° - 80°).

Crystallite size calculation using Scherrer's formula

$$D = \frac{K\lambda}{(\beta cos\theta)} \qquad \text{.....(3)}$$

Where,

D = The average crystallite size (nanometres or angstroms). This represents the dimension perpendicular to the diffracting planes.

K= Shape factor, stands for a geometrical factor that depends on crystallite apparent radius of gyration from the perspective of reflections

λ = Wavelength of X-ray

β = The full width at half maximum (FWHM) of a diffraction peak, also known as line broadening measured in radians.

θ = Bragg angle, which is half the 2θ angle at which the diffraction peak occurs.

The crystalline structure and phase composition of the synthesised nanomaterials were examined by X-ray diffraction (XRD) using Cu Kα radiation (λ = 1.5406 Å).

Step II: Field Emission Scanning Electron Microscope (FESEM)

FESEM is electron microscope that works by emitting electrons beam instead of light for scanning or imaging the sample. Coherent and bright electron beam generates by applying strong electric field to very sharp tungsten tip, then emitted electrons are accelerated and focused by series of electromagnetic lenses, which scanned across the sample surface in a raster pattern. The image is generated by capturing secondary electrons scattered from surface gives detailed information about the samples surface topography, and backscattered electrons which escape from deeper within the sample provides elemental composition and atomic number contrast. The detector captures the emitted electrons to form high resolution greyscale image after conversion. Its

Step III: Energy- Dispersive X-ray Spectroscopy (EDS)

EDS determines the elemental composition of sample by measuring the energy of X-rays emitted when the material is excited by an electron beam. When an electron beam

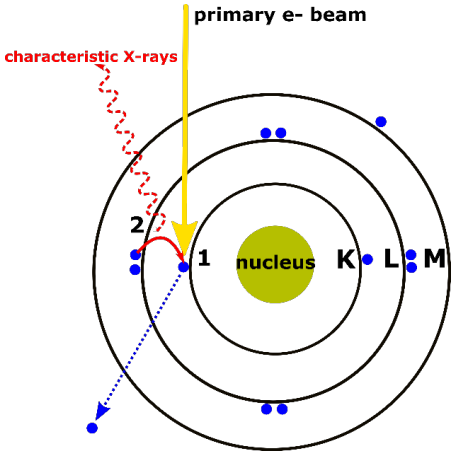

Figure 7. EDS spectroscopy

strikes the sample, it ejects the electron form sample atoms. Then to fill the vacancies, outer shell electrons fall into it, this process release energy in the form of X-rays. By

analysing peaks of spectrum at specific energies provide the elemental composition of sample. Hence it helps in identifying and quantifying the elements, elemental mapping for spatial distribution of nanomaterials.

4.2.6 Electrochemical Characterization

Step I: Pretreatment of Ni- Foam

Nickel foam was first cut into dimensions of 15 mm × 10 mm. To remove the native oxide layer, the foam was immersed in 3 M HCl solution and kept in an ultra sonicator for 30 minutes. After the acid treatment, the foam was immediately transferred to a beaker containing deionized (DI) water and rinsed 3–4 times to remove any residual acid. After thorough washing with DI water, the nickel foam was immersed in ethanol for 10 minutes to eliminate organic residues. Following this step, the foam was again rinsed 3–4 times with DI water to ensure complete removal of solvents. Finally, the cleaned nickel foam was dried in an oven at 60°C for 2 hours. Once dried, the pre-treated nickel foam was ready for drop casting with sample material for electrochemical testing.

Step II: Preparation of slurry for electrode coating

For the preparation of the working electrode, a slurry was prepared by first grinding 8 mg of the synthesized material, 1 mg of polyvinylidene fluoride (PVDF) as a binder, and 1 mg of activated carbon in dry state using an agate mortar and pestle. The mixture was dry ground slowly for 10–15 minutes to ensure uniform blending of the components. Next, 100 μL of isopropyl alcohol was added to the mixture, and grinding continued using the pestle until a uniform slurry was formed. The slurry was then diluted to a total volume of 1 mL and transferred into a vial, followed by sonication for 15 minutes to achieve better dispersion and prevent agglomeration.

Step III: Preparation of working electrode by drop casting method

A pre-cleansed nickel foam was placed flat and secured using a paper clip at in **Figure 8** to ensure stability during the casting process. The prepared slurry was then drop-cast onto the nickel foam drop by drop using a micropipette. Initially, two drops of the slurry were applied, and the electrode was dried in an oven at 60°C for 30 minutes before applying the next drops. This process was repeated until approximately 1 mL of slurry was uniformly deposited onto the nickel foam, and it made sure to cast in only 10 mm of nickel foam. After the final deposition, the coated electrode was dried at 60°C overnight in oven to ensure complete solvent removal and proper adhesion of the active material.

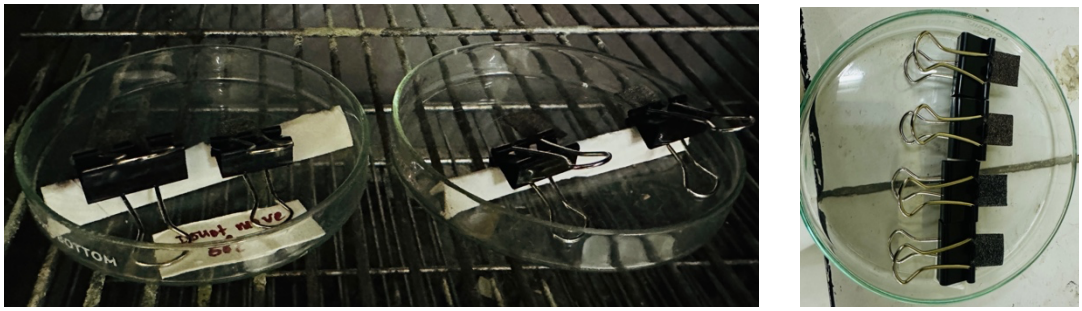

Figure 8. Electrode preparation

4.2.7 Electrochemical Characterization

Step I: Electrochemical setup

Once dried, the electrode was used as the working electrode (WE) in a three-electrode electrochemical setup, with a saturated Ag/AgCl electrode as the reference electrode (RE) and a platinum wire as the counter electrode (CE). A freshly prepared 6 M KOH aqueous solution was used as the electrolyte. Cyclic voltammetry (CV) was conducted within a voltage window of 0.0 – 0.45 V vs. Ag/AgCl at different scan rates (3 mVs^{-1}, 5, 10, 20, 30, 40, 50, 60, 70, 80, 90, 100 mVs^{-1}) to investigate the charge storage mechanism. Galvanostatic charge-discharge (GCD) test was recorded over 0 to 0.4 V vs. Ag/AgCl at 1 to 20 Ag^{-1} applied current density. Electrochemical impedance spectroscopy (EIS) measurement was measured in the frequency range 0.01 Hz to 1 x 10^5 Hz for all synthesized materials and also before and after cyclic stability test over 4000 GCD cycles.

Step II: Cyclic Voltammetry (CV)

The electrochemical workstation (potentiostat/ galvanostat) was initialized and the CV program was selected. Firstly, trial potential window for electrode material was tested for using 20 mVs^{-1} scan rate. Hence, after potential window identified, which was recorded to be 0 to 0.45 V, electrode was stabilized by performing CV test for 30 cycles in 20 mVs^{-1} scan rate. Then CV test data was recorded for potential scan rate from lower to the upper voltage limit (3 to 100 mVs^{-1}).

Step II: Galvanostatic Charge Discharge

For GCD test constant current was applied to the system to charge the electrode to the 0 to 0.4 V voltage range. Once the maximum voltage was reached, the current direction was reversed, and the electrode was discharged to the lower voltage limit. The voltage-time profiles during charging and discharging were recorded. GCD test were done in 1 Ag^{-1}, 2, 3, 4, 6, 8, 10, 15 and 20 Ag^{-1} current density. Every data are recorded and save as per the material used.

Step III: Electrochemical Impedance Spectroscopy (EIS)

Electrochemical impedance spectroscopy (EIS) is recorded by applying a small sinusoidal alternating current signal to an electrochemical system for measuring the voltage response over a range of frequencies (0.01 Hz to 100000 Hz). This plot gives the idea to analyse the capacitive behaviour, electrical resistance and the equivalent circuit of the electrochemical systems. This measurement at high frequencies captures fast processes of ohmic resistance while low frequencies capture slow processes or diffusion.

Impedance at each frequency is calculated using AC version of Ohm's law: $Z=E/I$, where E is potential and I is the current. The impedance is a complex number with both real part (resistive) and imaginary part (capacitive/inductive). The following equations is used to determine Impedance (Z) ((Magar et al., 2021)).

$$Z(\omega) = Z' + jZ'' \qquad \text{……..(4)}$$

Where,

ω ($2\pi f$) – angular frequency

Z′ – resistance

Z″ - reactance

Step IV: Cyclic Stability

In this experiment cyclic stability was done to evaluate the materials durability by repeating GCD and monitoring performance degradation over 4000 cycles. The decrease in capacitance value was evaluated. This helps in determining the materials lifespan and its ability to maintain performance over time. Only $ZnCo_2O4$ electrode was subject for GCD in 20 Ag^{-1}current for more than 4000 cycles. Initial EIS test was done before and final EIS test was also done to evaluate the change in impedance of electrode material over time.

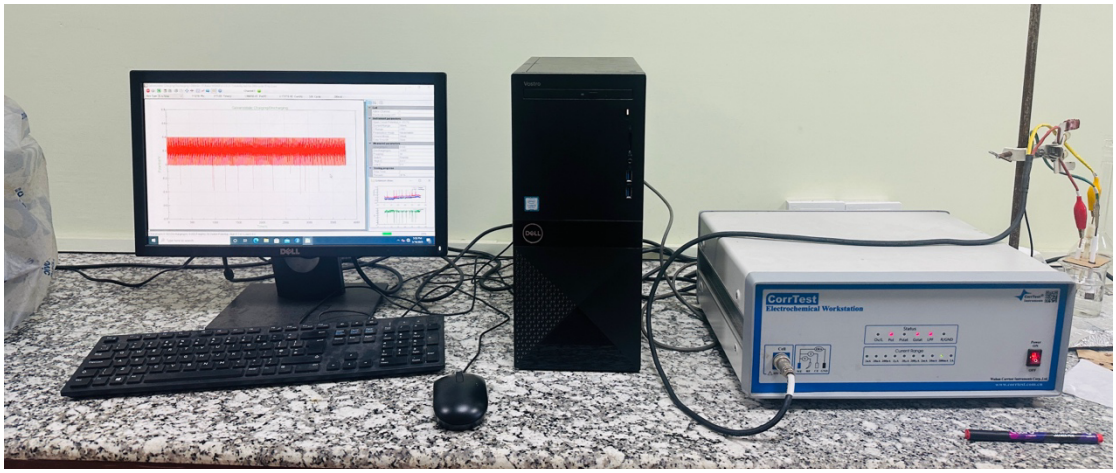

Figure 9. Electrochemical Workstation

CHAPTER 5: RESULTS AND DISCUSSION

5.1 X-ray Diffraction (XRD) analysis

a. $ZnCo_2O_4$

The characteristic diffraction peaks of $ZnCo_2O_4$ are observed at around **2θ ≈ 31.2°, 36.8°, 44.8°, 59.3°, and 65.2° in Figure 10**, which correspond to the (220), (311), (400), (511), and (440) planes, respectively which is assigned to spinel structure of $ZnCo_2O_4$ according to JCPDS card no. 23-1390. These results confirm the successful formation of $ZnCo_2O_4$ with a spinel crystalline phase. The average crystallite size (D) of $ZnCo_2O_4$ nanoparticles using the Debye- Scherrer equation (3) from the XRD pattern, analysing of the prominent peak 2θ ≈ 36.8° (FWHM ≈ 1.2 °) gives an expected to be in the nanometre range (~35nm), which aligns with the typical morphology of spinel $ZnCo_2O_4$.

b. $CoZn_2O_4$

The X-ray diffraction pattern of $CoZn_2O_4$ shows sharp peaks in **Figure 10**, which indicates crystalline nature of material. Here, the characteristics diffraction peaks are observed at 2θ values of ~**31.7°, 34.4°, 36.2°, 46.5°, 56.6°, 62.8°, and 68.0°**, which is indexed to the spinal-type cubic structure of $CoZn_2O_4$ according to JCPDS Card No. 23-1390. These reflections correspond to the (220), (311), (400), (422), (511), (440), and (533) crystallographic planes this confirms the successful formation of $CoZn_2O_4$ cubic spinel phase. The crystallite size of $CoZn_2O_4$ was calculated by using Debye-Scherrer equation (3), expected to be in the nanometre range of (~ 25 to 30 nm).

c. ZnO

X-ray diffraction (XRD) plot of the synthesized Zinc Oxide nanoparticles shows several sharp and intense peaks in **Figure 10** which confirm the crystalline nature of the nanomaterial. In figure major diffraction peaks for (2θ) at approximately 31.7°, 34.4°, 36.2°, 47.5°, 56.6°, 62.8°, 66.4°, 68.0°, and 69.1°, which correspond to the (100), (002), (101), (102), (110), (103), (200), (112), and (201) planes of the hexagonal wurtzite structure of ZnO, in good agreement with the standard JCPDS Card No. 36-1451 (PDF 89-1397). Also, sharpness and high intensity peaks indicate a well-crystallised nanomaterial. The average crystallite size of the ZnO nanoparticles was estimated using

the Debye–Scherrer equation, taking the most intense (101) peak at 2θ ≈ 36.2°. The calculated crystallite size was found to be in ~40 nm, confirming the nanocrystalline nature of the synthesized ZnO. Overall, the XRD results verify that the prepared sample is pure, single-phase ZnO with a hexagonal wurtzite structure and good crystallinity, suitable for further functional applications in supercapacitors.

d. CoO

In **Figure 10** major diffraction peaks are observed around 30.7°, 36.3°, 44°, and 65°. XRD plot with five hkl planes of Cobalt (II, III) Oxide (Co_3O_4) are (2 2 0), (3 1 1), (2 2 2) and (4 4 0) with standard JCPDS data card no (80- 1538). This shows Cobalt oxide in polycrystalline in nature. Lower intensity and peak broadening suggest smaller crystallite size with Cubic CoO structure with low crystallinity. Average crystallite size ranges from ~ 2- 4 nm ie. Nanocrystalline to amorphous.

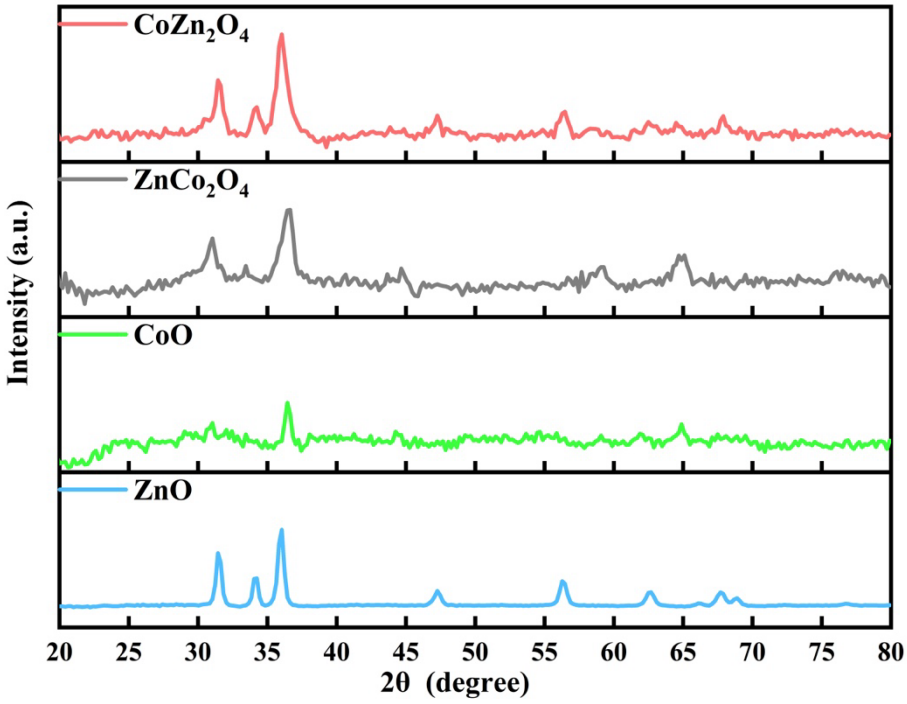

Figure 10. Comparative XRD spectra of CoO, ZnO, $CoZn_2O_4$ and $ZnCo_2O_4$

5.2 **Surface morphological study of $ZnCo_2O_4$ by SEM**

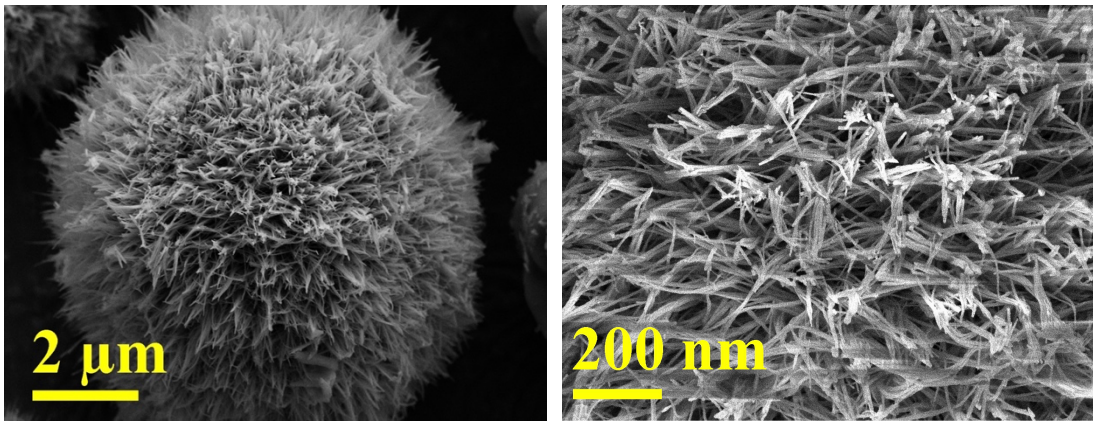

Figure 11. FE-SEM images of $ZnCo_2O_4$ microparticle and magnified

Low magnification image shows well defined spherical sea urchin like spherical microparticles. This hierarchical structure possessed of densely packed radially aligned needle-shaped projections. Nano needles are radiating outward form the central core. This 3-dimensional architecture demonstrates successful synthesis of highly organized morphology. This nano architecture provides a high surface- to- volume ratio which in electrochemical process facilitate efficient ion diffusion during charging and discharging process. Magnified image with nanoneedles structure with individual nanorod size 20-50nm in diameter and lengths extending to several hundred nanometres, significantly increase the specific surface area. This three-dimensional network forms abundant interstitial spaces and porous network, which creates open

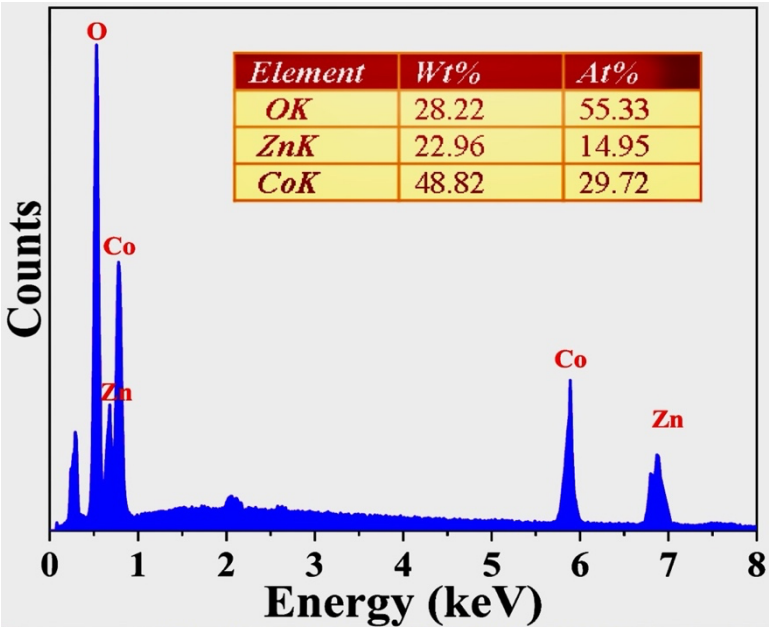

Figure 12. EDS spectra of $ZnCo_2O_4$ nanoparticles

channels for electrolyte penetration and enhance electrolyte accessibility and active site exposure, facilitating rapid electron transfer and increasing energy storage capacity of electrode material. The interconnected nature of the nanorods provides mechanical robustness which maintaining porosity, this improves the cyclic stability in electrochemical analysis. Also, this networked structure throughout the particle provide efficient electron transport pathways which reduced charge transfer resistance.

5.3 Elemental analysis of $ZnCo_2O_4$ by EDS

Figure 12 shows EDS of the $ZnCo_2O_4$ sample results distinct peaks for zinc, cobalt and oxygen with corresponding weight percentage of 22.96, 48.82, and 28.22% respectively. 48.82 % weight content of Cobalt confirms the stoichiometry (Zn: Co = 1:2) in $ZnCo_2O_4$. With atomic percentages of 55.33%, 14.95% and 29.72% of O: Zn: Co nearly matched with the expected ratio for $ZnCo_2O_4$, with theoretical atomic distribution is roughly O~ 57%, Zn~ 14% and Co~ 29%. This illustrates the successful synthesis of the spinel $ZnCo_2O_4$ phase with minimal impurities. Key EDS peaks of Co

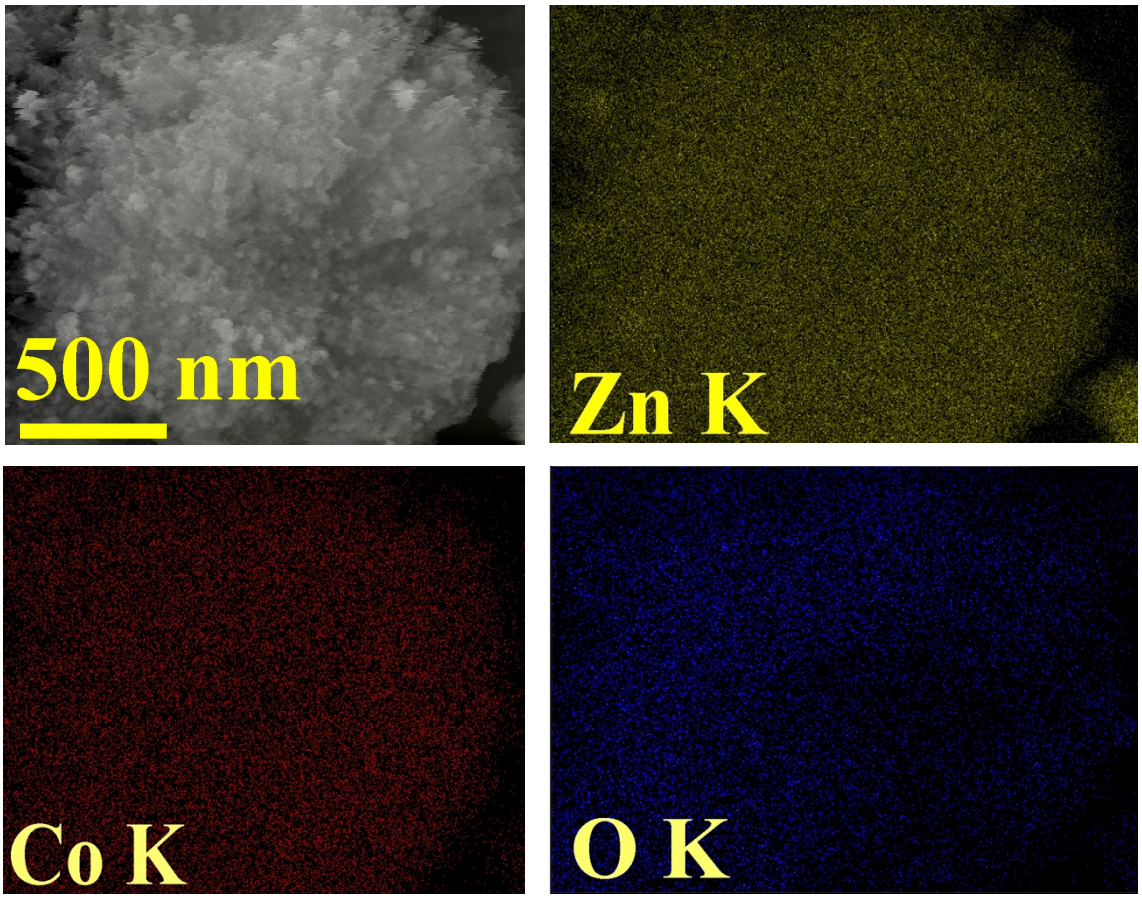

Figure 13. Elemental mapping of $ZnCo_2O_4$ nanoparticle

indicate cobalt rich regions with consistent with the Co^{2+} /Co^{3+}, which are redox- active centre in spinel structure. And lower intensity if Zn peaks indicated poor Zn content as expected for Zn- Co ratio 1:2. **Figure 13** shows elemental colour mapping of the $ZnCo_2O_4$ nano particles. This shows the distinct colours caused by Zinc, cobalt, and oxygen, which confirms the uniform spatial distribution of these elements across the nanoparticle. This shows excellent homogeneity of Zn, Co, and O throughout the nanoparticle, hence no phase separation, no elemental clustering.

5.4 Electrochemical analysis by Cyclic Voltammetry (CV)

To check the practical application potential of bimetallic oxide nanoparticle $ZnCo_2O_4$, $CoZn_2O_4$ charge storage performance was analysed in aqueous 6M KOH and compared with those of monometallic oxides ZnO and CoO in three three-electrode system. The electrochemical properties of $ZnCo_2O_4$, $CoZn_2O_4$, ZnO and CoO were evaluated using a three-electrode system in 6 M KOH electrolyte at room temperature. Cyclic voltammetry (CV) was conducted within a voltage window of 0.0 – 0.45 V vs. Ag/AgCl at different scan rates (3 mVs^{-1}, 5, 10, 20, 30, 40, 50, 60, 70, 80, 90, 100 mVs^{-1}) to investigate the charge storage mechanism. **Figure 14** presents a comparative CV profile of different synthesised oxides electrodes namely $ZnCo_2O_4$, $CoZn_2O_4$, ZnO and CoO in scan rate of 20mVs^{-1} with the potential range spanning from 0.0 to 0.45 V. All electrodes show redox peaks, indicating pseudocapacitive behaviour. Among them $ZnCo_2O_4$ exhibits the highest current response, both anodic and cathodic, which

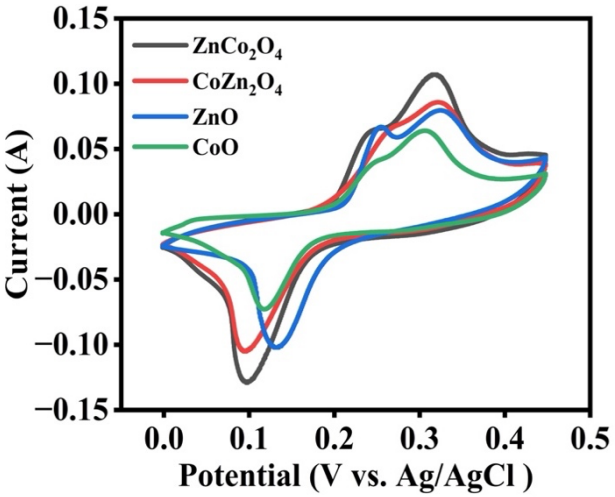

Figure 14. Comparative CV profile of $ZnCo_2O_4$, $CoZn_2O_4$, ZnO and CoO at scan rate 20mVs^{-1}

suggests a greater charge storage capacity. The higher current response of $ZnCo_2O_4$ indicates a larger electroactive surface area and better redox kinetics. Also, the distinct redox peaks around ~0.2 – 0.35 V correspond to Co^{2+}/Co^{3+} and Zn^{2+}/Zn^{3+} redox couples. This synergy between Zn and Co oxides in $ZnCo_2O_4$ enhances electron/ion transport and provide multiple oxidation states, improving overall capacitive behaviour. These observed redox peaks in $ZnCo_2O_4$ electrode, from battery like redox reactions of Zinc and Cobalt in the KOH electrolyte. $CoZn_2O_4$ also exhibits significant pseudocapacitive activity, but slightly less than $ZnCo_2O_4$. ZnO and CoO show smaller integrated areas, confirming their lower electrochemical activity due to fewer redox sites and limited conductivity.

Figure 15 (A) represents a comparative CV profile of $ZnCo_2O_4$ electrode with increase in the scan rates from 3 to 100 mVs^{-1} in the potential range of 0 to 0.45 V, shows the oxidation/ reduction peaks shift in response to increasing/ decreasing as the CV area increases. At higher scan rates the peaks and area increase due to polarization effects;

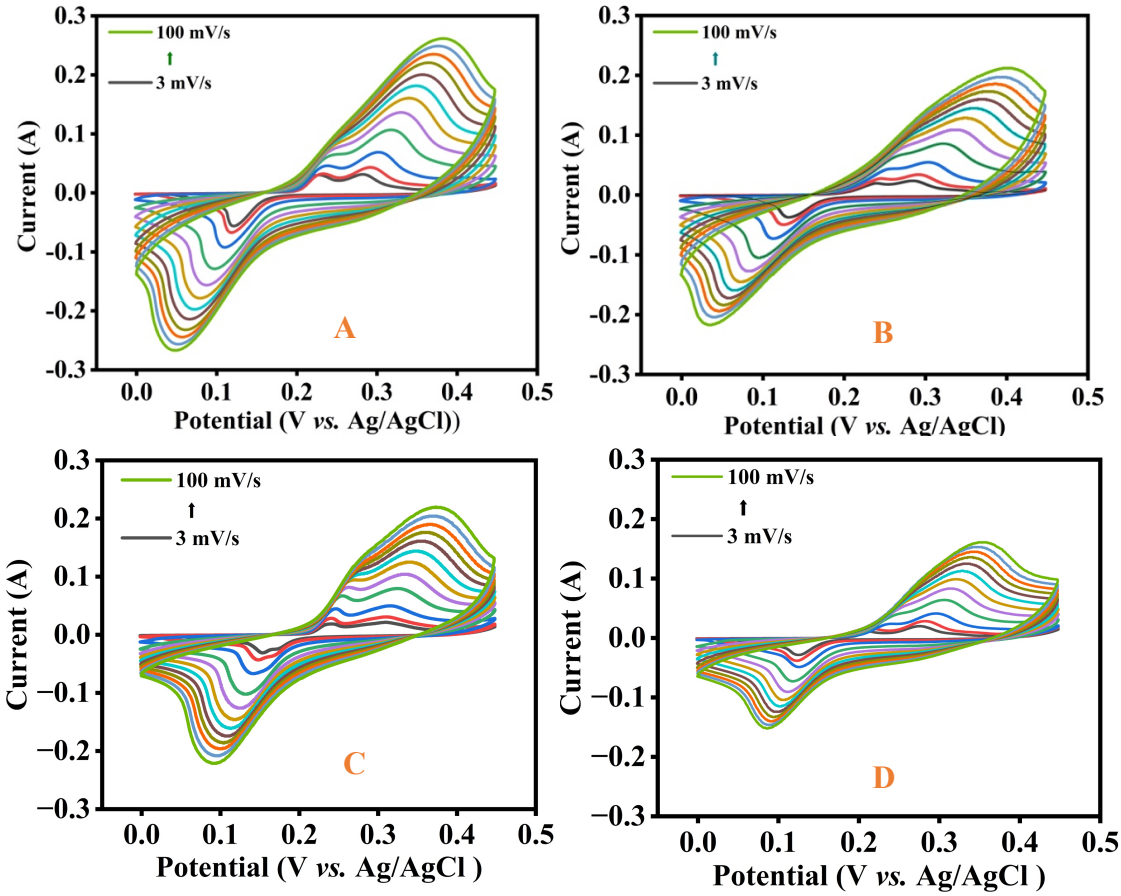

Figure 15. CV plots in different scan rates 3 to 100 mVs^{-1} (A) $ZnCo_2O_4$, (B) $CoZn_2O_4$, (C) ZnO, and (D) CoO

this happens due to the limited diffusion of ions to the electrode. Increasing scan rate causes reduction of time which are available for ion diffusion hampers their movement. Hence, when the scan rate is decreased, ions can completely utilize the available electroactive surface area for the diffusion, resulting in an increased charge storage capacity (Yewale et al., 2025a). This shift indicates increased internal resistance and slower ion diffusion at higher scan rates. Similar shift in shape and peak can be seen in

Figure 15 (B) for $CoZn_2O_4$ electrode with slightly smaller area under CV curves than that to $ZnCo_2O_4$ electrode. CV plots of ZnO and CoO are show in **Figure 15** (C) and (D) respectively, when the scan rate is increased from 3 to 100 mVs^{-1}, anodic peak shift toward positive potential and cathodic peak shift towards negative potential. This behaviour of every electrode indicates diffusion-controlled process having wider potential separation (Shrestha et al., 2018). This shift in faradaic redox peaks indicates the good electrochemical reversibility. The area under $ZnCo_2O_4$ electrode in different scan rate is higher than $CoZn_2O_4$ electrode sample, this indicates it shows higher energy storage capacity. Here both $ZnCo_2O_4$, and $CoZn_2O_4$ electrode material shows much better area under CV plots than that of ZnO and CoO electrodes. for ZnO two separate peaks seen in the CV plots, in alkaline media Zn can form soluble zincate and precipitated $Zn(OH)_2$, this creates separate oxidation features (Ko & Park, 2012). Similarly, for CoO multiple peaks is due to multiple oxidation states of cobalt (Liu et al., 2021). This verifies the bimetallic oxide electrode perform better compared to monometallic oxides in similar testing condition. Also, bimetallic oxide electrode shows synergistic faradaic electrochemical performance due to presence of two different metal constituents.

5.5 Electrochemical analysis by Galvanostatic charge-discharge (GCD)

Figure 16 provides insight of Galvanostatic charge-discharge (GCD) curves of oxides ($ZnCo_2O_4$, $CoZn_2O_4$, ZnO and CoO) recorded over 0 to 0.4 V vs. Ag/AgCl at $1Ag^{-1}$ applied current density. The charge-discharge curves displayed a nonlinear charging-

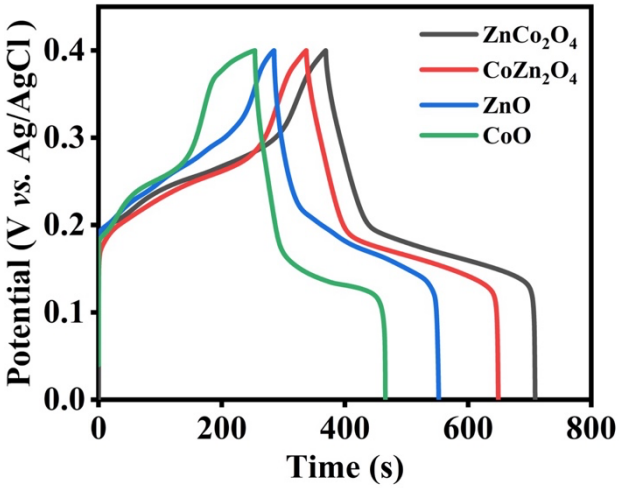

Figure 16. Comparative GCD profile of electrodes at 1 Ag^{-1} current density

discharging profile in the potential range with respect to time, and with a distinct plateau region, which indicates the confirmation of typical faradaic /pseudocapacitive redox behaviour due to the electrochemical adsorption and desorption of charge separation at the electrode and electrolyte interface. GCD profile of $ZnCo_2O_4$ with stoichiometric ratio 1:2 of precursor Zn salt and Co salt, shows the longest discharging time; this supports the higher specific capacitance value in compared to monometallic oxide. $CoZn_2O_4$ with a stoichiometric ratio 2:1 (Zinc salt to Cobalt salt) shows slightly shorter discharge duration, but still superior to single oxides. ZnO and CoO show a quick discharge duration, which indicates comparatively lower charge storage capacity. Also, the GCD curve obtained showed a consistent nature with respect to the CV analysis. The unsymmetrical charge-discharge behaviour is due to the certain kinetic irreversibility of OH^- ions of the electrolyte on the surface during the redox process (Meher et al., 2011).

Table 3. Comparative Specific Capacitance of different Oxides at 1 Ag^{-1} current density

SN	Electrode Material	Discharge time (s)	Current Density (Ag^{-1})	Potential (V)	Specific Capacitance (Fg^{-1})
1	$ZnCo_2O_4$	345.67	1	0.4	864.18
2	$CoZn_2O_4$	311.67	1	0.4	779.18
3	ZnO	267.37	1	0.4	668.43
4	CoO	209.07	1	0.4	522.68

Specific capacitances were calculated from GCD curves were which are presented in **Table 3**. Here the maximum value obtained by $ZnCo_2O_4$ nano particles electrode material compared with $CoZn_2O_4$, ZnO and Co_3O_4. this superior specific capacitance observed in bimetallic oxides, compared to their monometallic counterparts can be attributed to several synergistic factors. Bimetallic oxides combine the redox activity of two metal cations, enhancing faradaic pseudocapacitive behaviour. In the case of $ZnCo_2O_4$, both Zn^{2+} and Co^{3+}/Co^{2+} contribute to the charge storage process, enabling more efficient electrochemical reactions. Additionally, the presence of multiple oxidation states in cobalt facilitates rapid redox transitions, further improving capacitance. The spinel structure of $ZnCo_2O_4$ offers enhanced electrical conductivity due to electron hopping between Co ions and provides a stable framework that supports long-term cycling. Moreover, these materials often exhibit high surface area and porous nanostructures as indicated by SEM image, which allow for better electrolyte accessibility and ion diffusion. The combination of electrochemical activity, structural integrity, and efficient charge transport makes bimetallic oxides highly promising electrode materials for supercapacitor applications.

5.6 Study of specific capacitance of $ZnCo_2O_4$, $CoZn_2O_4$, ZnO, and CoO by varying current density:

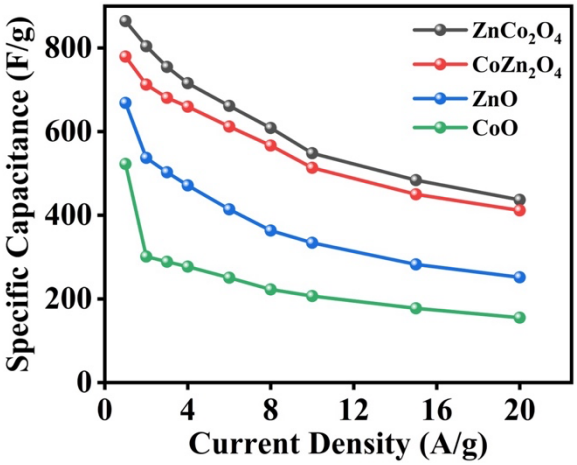

Figure 17. Comparative plot of specific capacitance vs. current density

Table 4. Rate capability performance of different oxides for current density 1 to 20 Ag^{-1}

		Specific Capacitance (Fg^{-1})			
Current Density (A/g)	**Potential window (V)**	**$ZnCo_2O_4$**	**$CoZn_2O_4$**	**ZnO**	**CoO**
1	0.4	864.17	779.17	668.42	522.67
2	0.4	804.0	712.35	537.00	301.17
3	0.4	754.5	680.75	502.75	288.75
4	0.4	715.6	659.66	471.33	277.00
6	0.4	661.5	612.0	414.00	250.50
8	0.4	608.6	566.66	363.33	222.67
10	0.4	548.33	513.33	334.17	206.67
15	0.4	483.75	450.0	282.50	177.50
20	0.4	436.67	411.66	251.67	155.00

	% retention	51%	53%	38%	30%

Figure 17 and **Table 4.** represents the rate capability performance of $ZnCo_2O_4$, $CoZn_2O_4$, ZnO and CoO electrodes, in which $ZnCo_2O_4$ electrode able to retain 51 % of specific capacitance i.e. from 864.18 Fg^{-1} to 436.67 Fg^{-1} when the current density increased to 20 Ag^{-1} from 1 Ag^{-1}, which illustrates good rate capability of nano particles of working electrode. Similarly, $CoZn_2O_4$ electrode retain 53% of initial specific capacitance at current density 20Ag^{-1}. But ZnO retain only 38% and CoO around 30% of their initial value at 20Ag^{-1} current density. This illustrates that bimetallic oxides have excellent rate capability compared to mono metallic oxides. The curve shows a monotonic decline, which is typical for pseudocapacitive materials. At higher current densities, ion diffusion becomes kinetically limited; i.e. only outer surface participates in charge storage, which ultimately leads to a lower capacitance.

5.7 Study of charge discharge profile of $ZnCo_2O_4$, $CoZn_2O_4$, ZnO, and CoO by varying current density

Figure 18 illustrates the GCD profiles of $ZnCo_2O_4$ electrode tested to current densities ranging from 1 to 10 Ag^{-1}. The $ZnCo_2O_4$ electrode exhibits wider discharge duration, this may be due to urchin-like structure of nanoparticles, this favours electron transport during oxidation and reduction processes occurring at time of charging and discharging cycles. The Cs, specific capacitance of each electrode was calculated by using equation 1.

$$Cs = \frac{I\,T}{\Delta m \Delta V} \qquad \text{……..(3)}$$

Where,

Cs = Specific Capacitance (Fg^{-1})

I = Current density (A)

T = Discharge time (s)

△m = Loading mass (g)

△V = Potential window (V)

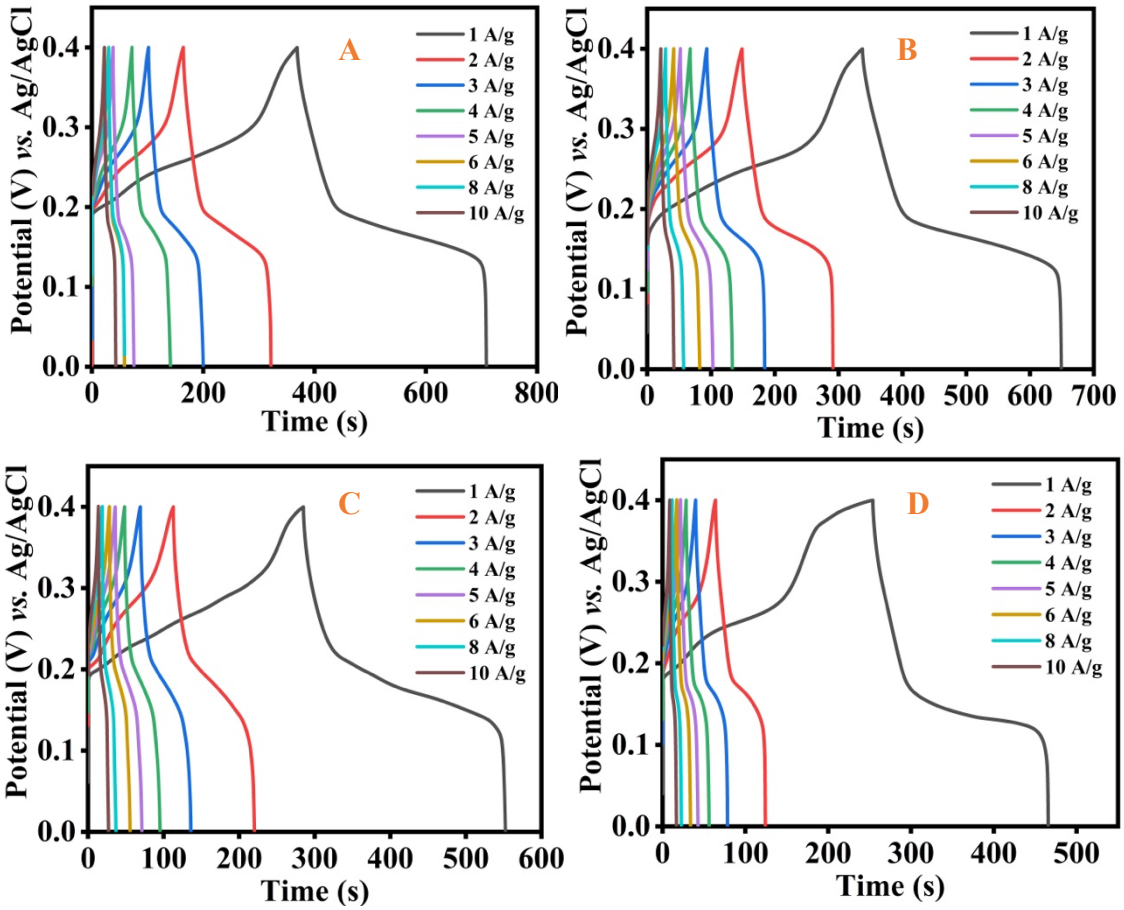

Figure 18. GCD plots of oxides (A) $ZnCo_2O_4$, (B) $CoZn_2O_4$, (C) ZnO, and (D) CoO

The GCD plots shows shortened discharge time with increasing current density i.e. specific capacitance decreases with increasing current. Characteristic plateau regions remain in every current but compress, this gives $ZnCo_2O_4$ retains the redox features and acceptable discharge shape even at high current, which indicates good rate capability/ fast kinetics relative to many pseudocapacitive materials. This further proof the synergistic effect between Zn and Co producing more electroactive sites and multiple accessible oxidation states. Figure 5. (D) shows the GCD plot of $CoZn_2O_4$ electrode at different current. Compare the $ZnCo_2O_4$ electrode, it shows slightly less discharge time in the same current and within same potential window of 0 to 0.4 V. This match with the CV plots of $CoZn_2O_4$ electrode in Figure 5. (C). i.e. $CoZn_2O_4$ electrode electrochemical performance is lower than that of $ZnCo_2O_4$ electrode with lower charge

storage capacity, lower specific capacitance. But both bimetallic oxide $ZnCo_2O_4$, and $CoZn_2O_4$ electrodes out perform in GCD plots for charging and discharging cycle compare with ZnO and CoO which are shown in Figure 18 (C) and (D) respectively. Both ZnO and CoO illustrate lower charging and discharging time duration compare to bimetallic oxides. among the 4 oxides CoO perform poorest in both CV and GCD plots, which confirms its weak electrochemical performance as electrode material for supercapacitor. This is due to faster electron transport in ZnO than CoO under similar testing condition. CoO with limited redox participation cause slow kinetics compared to moderate surface activity with better reversibility in ZnO. Hence in bimetallic oxides, combination of these elements overcomes the weaknesses in each other, like Zn enhances conductivity and ion diffusion, and Co provides rich redox sites and spinel structure offers high stability and porosity in electrode material.

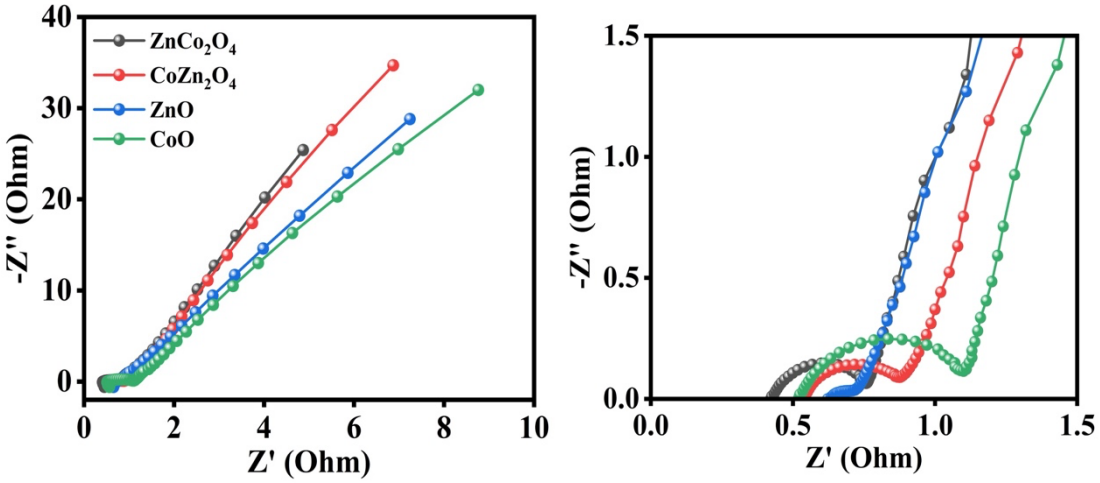

Figure 19. Comparative Nyquist plots of different electrodes with magnification

5.8 Electrochemical Impedance Spectroscopy (EIS) analysis

Figure 19 shows Nyquist plots of all samples, all curves display well well-defined semicircle in the high frequency region, followed by an inclined linear tail at the low-frequency region. This type of plot is a characteristic of a faradaic pseudocapacitive system governed by both charge-transfer and diffusion processes. The intercept on the real axis corresponds to the solution resistance (Rs), and the semicircle diameter represents the charge-transfer resistance (Rct). Among all, $ZnCo_2O_4$ shows the lowest Rct ~ 0.3 Ω, which signifies the rapid electron transport and enhanced redox activity, which is attributed to the synergistic interaction between Zn^{2+} and Co^{3+}/Co^{2+} centres. $CoZn_2O_4$ shows moderate semicircle radii with Rct value ~0.33 Ω, showing balanced

but comparatively slower kinetics than $ZnCo_2O_4$. Whereas, CoO exhibits the largest semicircle with Rct value ~ 0.52 Ω, this implies sluggish electron transport and poor electrochemical activity. Similarly at low-frequency tail region reflects Warburg impedance (Zw), $ZnCo_2O_4$ shows steeper line, confirming better ion diffusion and capacitive behaviour. Hence, EIS results correlate with the specific capacitance trend, which further confirms that bimetallic oxide $ZnCo_2O_4$ provides the most efficient charge-storage dynamics due to its mixed- valence redox activity and enhanced conductivity.

5.9 Study of $ZnCo_2O_4$ electrode Cyclic Stability

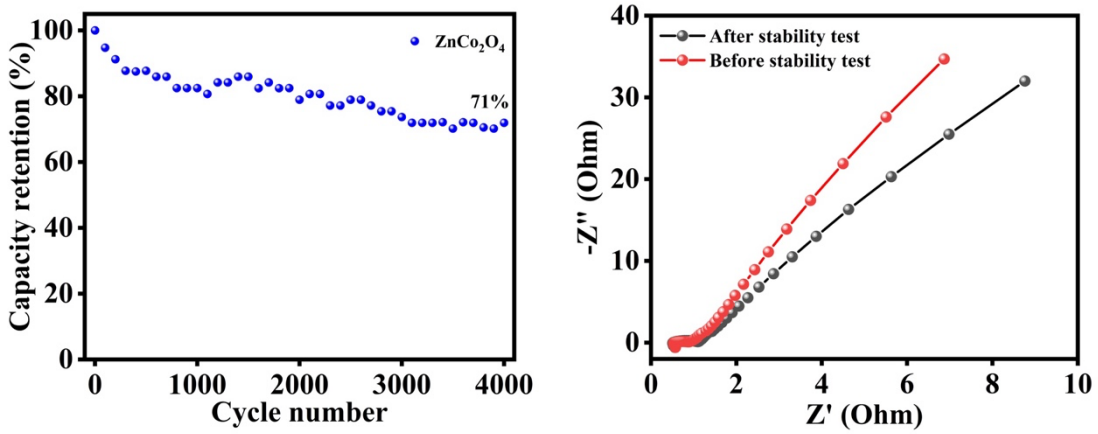

Figure 20. Plot of capacity retention percentage vs. GCD cycle for $ZnCo_2O_4$ electrode and EIS plot before and after cyclic stabilty test for 4000 GCD cycles

For cyclic stability of electrode material, electrode was test for more than 4000 GCD cycles. **Figure 21** shows cyclic stability of $ZnCo_2O_4$ electrode material, electrode was subjected to long-term cyclic stability testing for over 4000 GCD cycles. It exhibits 71% of retention after 4000 cycles at higher current density of 20 Ag^{-1}, which helps in evaluating the practical applicability in superconductor electrode. The capacity retention gradually declines for initial 500 cycles likely caused by the structural rearrangement or some electrode pulverization, formation of a stable electrode-electrolyte interface, or due to loss of electroactive material due to mechanical stress and dissolution. In mid- region (500- 3000 cycles) specific capacitance retention stays relatively steady (~80- 75%), this indicates the robust structure with stable ion diffusion paths, good electrical contact and stable faradaic and capacitive contributions. And the final decay after 3000 cycles may suggest slow degradation of the active surface due to

fatigue from repeated redox reactions and continuous volume expansion/ contraction. EIS spectra of $ZnCo_2O_4$ electrode obtained before and after the cyclic stability test, plot shows semicircle region increases after cycling that is small rise in Rct, and straight line at low frequency/ Warburg slope shows near parallel indicating retained ion diffusion and capacitive nature after cycling. This increase in Rct suggests minor surface or interface deterioration, this explains loss of capacity. And unchanged Rs ie identical low- frequency slope supports ion diffusion and electrolyte conductivity through pores remain intact. This combination of stable EIS behaviour and strong cycling retention illustrates $ZnCo_2O_4$ as a promising electrode material for supercapacitor applications.

5.10 Comparative study of Specific Capacitance of $ZnCo_2O_4$ with literature values

Table 5. The specific capacitance of $ZnCo_2O_4$ nano-structure comparison with previous recorded works.

Morphology	**Synthesis**	**Specific Capacitance (Fg^{-1})**	**Reference**
Porous quasi-cubes	Solvothermal – calcination	804 (1 Ag^{-1})	(Chen et al., 2020)
Nanoparticles	MOF- calcination	457 (1 Ag^{-1})	(Chen et al., 2015)
Nanowires	Hydrothermal-calcination	776.2 (1 Ag^{-1})	(Xu et al., 2017)
Nanoparticles	Hydrothermal-calcination	635 (7 $mAcm^{-2}$)	(Yewale et al., 2025b)
Nanoparticles	Hydrothermal-calcination	864.18 (1 Ag^{-1})	This work

Similar recorded works done on $ZnCo_2O_4$ as electrode material show in table 5, electrochemical performance of synthesised nanomaterial in this research work is better than similar works. Synthesis method and procedure used in this research seem better compared to the previous recorded works. Material used, temperature of hydrothermal and calcination somehow effects the morphology and structure of nanomaterial which ultimately effects the electrochemical properties of the electrode.

CHAPTER 6: CONCLUSION AND RECOMMENDATIONS

6.1 Conclusions

Hence in summary, in this research transition metal bimetallic oxides were successfully synthesised by using facile hydrothermal process followed by inert atmospheric calcination in tube furnace. These synthesised materials were verified structurally i.e. after calcination crystal material sample is formed by XRD test and for morphology of sample FESEM imaging done which shows the urchin like particle shape with densely packed nanoflakes radiating outward. The EDS test confirms the elemental composition and homogeneity of sample materials. And electrochemical characterization investigates the electrochemical performance of $ZnCo_2O_4$ nano particles. $ZnCo_2O_4$ electrode achieved superior specific capacitance 864.18 F g^{-1} at 1Ag^{-1} current density better than $CoZn_2O_4$ and superior to mono metallic oxides ZnO and CoO. The stable CV profiles at high scan rates confirm good rate capability and reversible charge-discharge behavior desirable for supercapacitor application. It retains nearly 51% of initial specific capacitance at higher 20 Ag^{-1} current, which signifies robust structural stability and good cycling stability of 71% retention at current 20Ag^{-1} after 4000 cycles. The XRD patterns confirm the successful synthesis of pure $ZnCo_2O_4$, homogenous spinel phase and enhance crystallinity with nanostructured sea urchin like morphology suited for electrochemical energy storage. The EIS analysis confirms $ZnCo_2O_4$ electrode exhibits low internal resistance with Rct ~0.3 Ω, fast charge transfer kinetics, near 45º Warburg impedance at low frequency region for efficient ion diffusion and dominant capacitive behaviour. The electrochemical performance of $ZnCo_2O_4$ material is better than previously recorded data. Hence, the synthetic method is a simple operation, cost-saving, and efficient, and can be extended to the preparation of bimetallic oxide electrode materials with notable electrochemical performance for their real applications in the field of advanced energy storage solutions.

6.2 Recommendations:

For improvement in the process of synthesis of precursor material for supercapacitor electrode, several suggestions can be offered:

- Optimization of synthesis parameters, such as calcination temperature and precursor ratios, to further enhance electrochemical performance.

- Investigation of different electrolytes (e.g., ionic liquids or organic electrolytes) for extended voltage windows and higher energy density.
- Integration of $ZnCo_2O_4$ with carbon-based materials (e.g., graphene, carbon nanotubes) to improve conductivity and cycling stability.
- Exploration of asymmetric and hybrid supercapacitor configurations to achieve higher energy density.
- Hence, further research and optimization could enable its practical implementation in commercial supercapacitors.

References

1. Abbasi, K., Jiao, Z., Shahbaz, M., & Khan, A. (2020). Asymmetric impact of renewable and non-renewable energy on economic growth in Pakistan: New evidence from a nonlinear analysis. *Energy Exploration & Exploitation*, *38*(5), 1946-1967.

2. Al-Obaidi, A., & NguyenHuynh, T. (2018). Renewable vs. conventional energy: which wins the race to sustainable development? IOP Conference Series: Materials Science and Engineering,

3. Anandharamakrishnan, C. (2013). Characterization of Nanoparticles. *Techniques for nanoencapsulation of food ingredients*, 65-67.

4. Askari, M. B., Salarizadeh, P., Beheshti-Marnani, A., & Di Bartolomeo, A. (2021). NiO-Co3O4-rGO as an efficient electrode material for supercapacitors and direct alcoholic fuel cells. *Advanced Materials Interfaces*, *8*(15), 2100149.

5. Balaji, T. E., Tanaya Das, H., & Maiyalagan, T. (2021). Recent trends in bimetallic oxides and their composites as electrode materials for supercapacitor applications. *ChemElectroChem*, *8*(10), 1723-1746.

6. Biswas, P., Rashid, A., Biswas, A., Nasim, M. A. A., Chakraborty, S., Gupta, K. D., & George, R. (2024). AI-driven approaches for optimizing power consumption: a comprehensive survey. *Discover Artificial Intelligence*, *4*(1), 116.

7. Chen, H., Du, X., Sun, J., Mao, H., Wu, R., & Xu, C. (2020). Simple preparation of ZnCo2O4 porous quasi-cubes for high performance asymmetric supercapacitors. *Applied Surface Science*, *515*, 146008.

8. Chen, S., Xue, M., Li, Y., Pan, Y., Zhu, L., Zhang, D., Fang, Q., & Qiu, S. (2015). Porous ZnCo 2 O 4 nanoparticles derived from a new mixed-metal organic framework for supercapacitors. *Inorganic Chemistry Frontiers*, *2*(2), 177-183.

9. Gan, Y. X., Jayatissa, A. H., Yu, Z., Chen, X., & Li, M. (2020). Hydrothermal synthesis of nanomaterials. *Journal of Nanomaterials*, *2020*.

10. Gogotsi, Y., & Penner, R. M. (2018). Energy storage in nanomaterials–capacitive, pseudocapacitive, or battery-like? In (Vol. 12, pp. 2081-2083): ACS Publications.

11. Gonçalves, J. M., da Silva, M. I., Silva, M. N., Martins, P. R., Nossol, E., Toma, H. E., & Angnes, L. (2022). Recent progress in ZnCo 2 O 4 and its composites for energy storage and conversion: a review. *Energy Advances*, *1*(11), 793-841.

12. González, A., Goikolea, E., Barrena, J. A., & Mysyk, R. (2016). Review on supercapacitors: Technologies and materials. *Renewable and sustainable energy reviews*, *58*, 1189-1206.

13. Iro, Z. S., Subramani, C., & Dash, S. (2016). A brief review on electrode materials for supercapacitor. *International Journal of Electrochemical Science*, *11*(12), 10628-10643.

14. Khan, I. A., Thekkekara, L., Waqar, S., Choudhry, N., & John, S. (2021). *Supercapacitors fabrication and performance evaluation techniques*. IntechOpen.

15. Ko, Y., & Park, S.-M. (2012). Zinc oxidation in dilute alkaline solutions studied by real-time electrochemical impedance spectroscopy. *The Journal of Physical Chemistry C*, *116*(13), 7260-7268.

16. Kumar, Y. A., Roy, N., Ramachandran, T., Hussien, M., Moniruzzaman, M., & Joo, S. W. (2024). Shaping the future of energy: The rise of supercapacitors progress in the last five years. *Journal of Energy Storage*, *98*, 113040.

17. Lalwani, S., Munjal, M., Singh, G., & Sharma, R. K. (2019). Layered nanoblades of iron cobaltite for high performance asymmetric supercapacitors. *Applied Surface Science*, *476*, 1025-1034.

18. Liu, J., Wang, J., Xu, C., Jiang, H., Li, C., Zhang, L., Lin, J., & Shen, Z. X. (2018). Advanced energy storage devices: basic principles, analytical methods, and rational materials design. *Advanced science*, *5*(1), 1700322.

19. Liu, W., Zhang, Z., Zhang, Y., Zheng, Y., Liu, N., Su, J., & Gao, Y. (2021). Interior and exterior decoration of transition metal oxide through Cu0/Cu+ Co-doping strategy for high-performance supercapacitor. *Nano-micro letters*, *13*(1), 61.

20. Liu, X., Li, Q., Qin, Y., & Jiang, Y. (2020). Constructing high-performance electrode materials using core–shell ZnCo 2 O 4@ PPy nanowires for hybrid batteries and water splitting. *Rsc Advances*, *10*(47), 28324-28331.

21. Liu, Y., Wen, S., & Shi, W. (2018). Co3S4 nanoneedles decorated on NiCo2O4 nanosheets for high-performance asymmetric supercapacitors. *Materials Letters*, *214*, 194-197.

22. Lokhande, P. E., Chavan, U. S., & Pandey, A. (2020). Materials and fabrication methods for electrochemical supercapacitors: overview. *Electrochemical Energy Reviews*, *3*, 155-186.

23. Magar, H. S., Hassan, R. Y., & Mulchandani, A. (2021). Electrochemical impedance spectroscopy (EIS): Principles, construction, and biosensing applications. *Sensors*, *21*(19), 6578.

24. Mayeen, A., Shaji, L. K., Nair, A. K., & Kalarikkal, N. (2018). Morphological Characterization of Nanomaterials. *Characterization of nanomaterials* 335-364. (Woodhead Publishing)

25. Meher, S. K., Justin, P., & Rao, G. R. (2011). Nanoscale morphology dependent pseudocapacitance of NiO: Influence of intercalating anions during synthesis. *Nanoscale*, *3*(2), 683-692.

26. Mendhe, A., & Panda, H. (2023). A review on electrolytes for supercapacitor device. *Discover Materials*, *3*(1), 29.

27. Molahalli, V., Sharma, A., Bijapur, K., Soman, G., Chattham, N., & Hegde, G. (2024). Low-cost bio-waste carbon nanocomposites for sustainable electrochemical devices: A systematic review. *Materials Today Communications*, *38*, 108034.

28. Pawar, S. A., Yu, S., Ju, E., Seo, H., Yeu, J., Kim, J., Patil, D. S., & Shin, J. C. (2019). Zinc cobalt layered double hydroxide electrode for high-performance supercapacitor. *Applied Science and Convergence Technology*, *28*(5), 164-168.

29. Prabhakar Vattikuti, S. V., Shim, J., Rosaiah, P., Mauger, A., & Julien, C. M. (2023). Recent advances and strategies in MXene-based electrodes for supercapacitors: applications, challenges and future prospects. *Nanomaterials*, *14*(1), 62.

30. Rudra, S., Seo, H. W., Sarker, S., & Kim, D. M. (2024). Supercapatteries as hybrid electrochemical energy storage devices: current status and future prospects. *Molecules*, *29*(1), 243.

31. Shi, F., Li, L., Wang, X.-l., Gu, C.-d., & Tu, J.-p. (2014). Metal oxide/hydroxide-based materials for supercapacitors. *Rsc Advances*, *4*(79), 41910-41921.

32. Shrestha, K. R., Kandula, S., Rajeshkhanna, G., Srivastava, M., Kim, N. H., & Lee, J. H. (2018). An advanced sandwich-type architecture of MnCo 2 O 4@ N–C@ MnO 2 as an efficient electrode material for a high-energy density hybrid asymmetric solid-state supercapacitor. *Journal of Materials Chemistry A*, *6*(47), 24509-24522.

33. Sun, H., Miao, Y., Wang, G., Han, X., Xu, C., Zhu, J., & Chen, H. (2024). Battery-type ZnCo2O4 nanosheets and nanowires as advanced cathode materials for hybrid supercapacitors with ultra-long cycling stability. *Journal of Energy Storage*, *92*, 112189.

34. Tiwari, N., Kadam, S., & Kulkarni, S. (2021). Synthesis and characterization of ZnCo2O4 electrode for high-performance supercapacitor application. *Materials Letters*, *298*, 130039.

35. Vangari, M., Pryor, T., & Jiang, L. (2013). Supercapacitors: review of materials and fabrication methods. *Journal of energy engineering*, *139*(2), 72-79.

36. Xu, L., Zhao, Y., Lian, J., Xu, Y., Bao, J., Qiu, J., Xu, L., Xu, H., Hua, M., & Li, H. (2017). Morphology controlled preparation of ZnCo2O4 nanostructures for asymmetric supercapacitor with ultrahigh energy density. *Energy*, *123*, 296-304.

37. Yewale, M. A., Desarada, S. V., Teli, A. M., Chavan, K. B., Morankar, P. J., Shin, D. K., & Choi, S. T. (2025a). Synthesis of the ZnCo2O4 positive electrode using a urea-assisted hydrothermal approach for supercapacitor applications. *Energy & Fuels*, *39*(4), 2281-2293.

38. Yewale, M. A., Desarada, S. V., Teli, A. M., Chavan, K. B., Morankar, P. J., Shin, D. K., & Choi, S. T. (2025b). Synthesis of the ZnCo2O4 Positive Electrode Using a Urea-Assisted Hydrothermal Approach for Supercapacitor Applications. *Energy & Fuels*.

39. Zameer, A., Jaffar, F., Shahid, F., Muneeb, M., Khan, R., & Nasir, R. (2023). Short-term solar energy forecasting: Integrated computational intelligence of LSTMs and GRU. *Plos one*, *18*(10), e0285410.

40. Zeghlouli, J., Christophe, G., Guendouz, A., El Modafar, C., Belkamel, A., Michaud, P., & Delattre, C. (2021). Optimization of bioethanol production from enzymatic treatment of Argan pulp feedstock. *Molecules*, *26*(9), 2516.

41. Zhang, Y., Feng, H., Wu, X., Wang, L., Zhang, A., Xia, T., Dong, H., Li, X., & Zhang, L. (2009). Progress of electrochemical capacitor electrode materials: A review. *International Journal of Hydrogen Energy*, *34*(11), 4889-4899.

42. Zhi, M., Xiang, C., Li, J., Li, M., & Wu, N. (2013). Nanostructured carbon–metal oxide composite electrodes for supercapacitors: a review. *Nanoscale*, *5*(1), 72-88.

17% Overall Similarity

The combined total of all matches, including overlapping sources, for each database.

Filtered from the Report

- Bibliography
- Quoted Text
- Small Matches (less than 10 words)
- Abstract

Custom Section Exclusions

{titlesCount} Section Titles, {keywordsCount} Keywords

Section title	No. of Section Starters	Section Starters
"Acknowledgements"	4	Acknowledgements, Acknowledgement, Acknowledgment, Acknowledgments

Match Groups

- **113** Not Cited or Quoted 14%
  Matches with neither in-text citation nor quotation marks
- **22** Missing Quotations 3%
  Matches that are still very similar to source material
- **0** Missing Citation 0%
  Matches that have quotation marks, but no in-text citation
- **0** Cited and Quoted 0%
  Matches with in-text citation present, but no quotation marks

Top Sources

14% Internet sources
10% Publications
0% Submitted works (Student Papers)

Integrity Flags

0 Integrity Flags for Review

No suspicious text manipulations found.

Our system's algorithms look deeply at a document for any inconsistencies that would set it apart from a normal submission. If we notice something strange, we flag it for you to review.

A Flag is not necessarily an indicator of a problem. However, we'd recommend you focus your attention there for further review.

Pulchowk Campus
Institute of Engineering
Tribhuvan University

RABIN CHAKATU <079msmse012.rabin@pcampus.edu.np>

Fwd: About Revision of Manuscript Based on Reviewer Comments (Manuscript ID: ARJ_V6_2025_C27)

4 messages

Khemraj Shrestha <chemkhem@gmail.com> Mon, Dec 8, 2025 at 2:36 PM
To: RABIN CHAKATU <079msmse012.rabin@pcampus.edu.np>

2040

---------- Forwarded message ---------
From: <arj@amritcampus.edu.np>
Date: Mon, Dec 8, 2025 at 2:28 PM
Subject: About Revision of Manuscript Based on Reviewer Comments (Manuscript ID: ARJ_V6_2025_C27)
To: <chemkhem@gmail.com>, Swagatstha <swagatstha@gmail.com>

Dear authors,

Thank you for submitting your manuscript entitled “SYNTHESIS AND ELECTROCHEMICAL CHARACTERISATION OF ZINC COBALT BIMETALLIC OXIDE AS AN ADVANCED POSITRODE MATERIAL FOR SUPERCAPACITOR APPLICATION (Manuscript ID: ARJ_V6_2025_C27)” to Amrit Research Journal (ARJ).

The peer-review process has now been completed, and the reviewers have provided their comments and suggestions for improvement. Therefore, your paper is acceptable for publication after the minor revision of the manuscript. We kindly request you to revise your manuscript by addressing all the reviewers’ comments point-by-point, and clearly indicating the changes made in the revised document. Also, please review the plagiarism report and make the necessary corrections to ensure compliance with the journal’s originality requirements.

Please ensure that:
1. The manuscript strictly follows the ARJ Author Guidelines.
2. The referencing style is carefully corrected according to the journal’s required format (i.e., APA 7th Edition).
3. A separate response letter is included, explaining how each comment has been addressed.

We request you to return the revised manuscript and response letter within 7 days of this email.
Once we receive your revised manuscript, we will review the changes and proceed with the further editorial decision process.

We appreciate your cooperation and look forward to receiving the revised version soon.

Warm regards,
Assoc. Prof. Dr. Swagat Shrestha
Chief Editor
Amrit Research Journal (ARJ)

Amrit Campus, Tribhuvan University
Lainchaur, Kathmandu, Nepal
Email: swagatstha@gmail.com